J Neurophysiol 121: 1879–1895, 2019.
First published February 27, 2019; doi:10.1152/jn.00869.2016.

RESEARCH ARTICLE | *Sensory Processing*

Quantification of vibrissal mechanical properties across the rat mystacial pad

Anne En-Tzu Yang,[1] Hayley M. Belli,[2] and Mitra J. Z. Hartmann[1,2]
[1]*Department of Mechanical Engineering, Northwestern University, Evanston, Illinois; and* [2]*Department of Biomedical Engineering, Northwestern University, Evanston, Illinois*

Submitted 8 November 2016; accepted in final form 25 February 2019

Yang AE, Belli HM, Hartmann MJ. Quantification of vibrissal mechanical properties across the rat mystacial pad. *J Neurophysiol* 121: 1879–1895, 2019. First published February 27, 2019; doi: 10.1152/jn.00869.2016.—Recent work has quantified the geometric parameters of individual rat vibrissae (whiskers) and developed equations that describe how these parameters vary as a function of row and column position across the array. This characterization included a detailed quantification of whisker base diameter and arc length as well as the geometry of the whisker medulla. The present study now uses these equations for whisker geometry to quantify several properties of the whisker that govern its mechanical behavior. We first show that the average density of a whisker is lower in its proximal region than in its distal region. This density variation appears to be largely attributable to the presence of the whisker cuticle rather than the medulla. The density variation has very little effect on the center of mass of the whisker. We next show that the presence of the medulla decreases the deflection of the whisker under its own weight and also decreases its mass moment of inertia while sacrificing $<1\%$ stiffness at the whisker base compared with a solid whisker. Finally, we quantify two dimensionless parameters across the array. First, the deflection-to-length ratio decreases from caudal to rostral: caudal whiskers are longer but deflect more under their own weight. Second, the nondimensionalized radius of gyration is approximately constant across the array, which may simplify control of whisking by the intrinsic muscles. We anticipate that future work will exploit the mechanical properties computed in the present study to improve simulations of the mechanosensory signals associated with vibrissotactile exploratory behavior.

NEW & NOTEWORTHY The mechanical signals transmitted by a whisker depend critically on its geometry. We used measurements of whisker geometry and mass to quantify the center of mass, mass moment of inertia, radius of gyration, and deflection under gravity of the whisker. We describe how variations in these quantities across the array could enhance sensing behaviors while reducing energy costs and simplifying whisking control. Most importantly, we provide derivations for these quantities for use in future simulation work.

active sensing; behavior; touch; trigeminal; whisker

INTRODUCTION

During tactile exploratory behavior, rats often oscillate their vibrissae (whiskers) back and forth at frequencies between 5 and 25 Hz in a behavior known as "whisking" (Berg and Kleinfeld 2003; Vincent 1912; Welker 1964; Wineski 1983). With the use of only mechanical information from its whiskers, a rat can determine the location, size, orientation, and texture of an object (Brecht et al. 1997; Carvell and Simons 1990; Diamond 2010; Guić-Robles et al. 1989; Knutsen et al. 2006; Polley et al. 2005; Yang and Hartmann 2016). The rat vibrissal-trigeminal system has, therefore, become an important model for the study of active sensing, that is, for investigating the effects of movement and mechanics on the sensory data received (Ahissar and Kleinfeld 2003; Bosman et al. 2011; Bush et al. 2016b).

The mechanical signals transmitted during whisking behavior depend critically on whisker geometry. In a recent study, we (Belli et al. 2017) quantified whisker geometry as a function of the row and column position within the array, including arc length, base diameter, medulla geometry, radius ratio, and radius slope. This geometry will affect the quasistatic bending of the whisker as well as its dynamic response (Adineh et al. 2015; Boubenec et al. 2012; Hartmann 2015; Kan et al. 2013; Lucianna et al. 2016).

The quasistatic bending of the whisker governs the mechanosensory signals that the rat will obtain as the whiskers deform when they press against objects (Birdwell et al. 2007; Hires et al. 2013, 2016; Huet et al. 2015; Huet and Hartmann 2016; Kaneko et al. 1998; Kim and Moller 2007; Quist and Hartmann 2012; Solomon and Hartmann 2006, 2010, 2011; Ueno et al. 1998; Yang and Hartmann 2016). Under quasistatic assumptions, in which the effects of time and inertia are irrelevant, only the geometry of the whisker and its elastic properties (Young's modulus and Poisson's ratio) influence how an external force is transmitted to the vibrissal base. In other words, the quasistatic response of a whisker to an external input depends solely on its geometry and elastic (material) properties.

In contrast, the dynamic response of the whisker refers to the mechanosensory signals governed by its mass and inertia in response to force, torque, or change in state (Boubenec et al. 2012; Hires et al. 2016; Kan et al. 2013; Quist et al. 2014; Vaxenburg et al. 2018). Whisker dynamics are especially important when quantifying noncontact whisking, the collision generated at the instant the whisker contacts an object, and whisker vibrations. The dynamic response of a whisker depends not only on its geometry and elastic properties, but also on its inertial properties, which characterize its mass distribution.

In the present work, we use the equations for average whisker geometry developed in Belli et al. (2017) along with

Address for reprint requests and other correspondence: M. J. Z. Hartmann, Mechanical Engineering Dept., Northwestern Univ., 2145 Sheridan Rd., Evanston, IL 60208 (e-mail: hartmann@northwestern.edu).

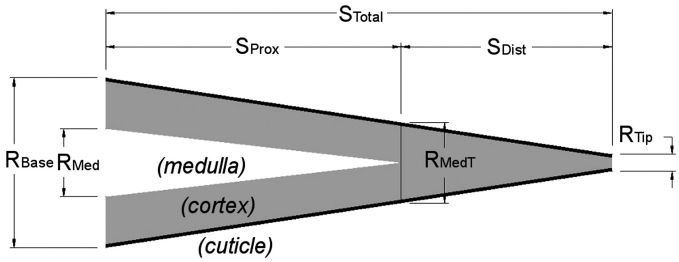

Fig. 1. Schematic of the structural elements of the whisker. Whisker is modeled with base radius R_{Base} and tip radius R_{Tip}. Medulla is defined as a hollow cone with negligible tip diameter. Radius of the medulla at its base is denoted by R_{Med}, and the radius of the whisker at medulla termination point, R_{MedT}. Total whisker arc length (S_{Total}) can be broken into proximal (S_{Prox}), occupied by the medulla, and distal (S_{Dist}). Note that the schematic is not to scale.

mass measurements to quantify several mechanical properties of the whiskers. An important motivation for the present study is to lay the groundwork for future simulations that will require accurate descriptions of how whisker mechanical parameters vary across the array. In addition, we specifically tested the hypotheses that the whisker geometry would *1*) reduce the deflection of the whisker under its own weight for a given whisker length and *2*) reduce the amount of energy required to whisk at a given rotational velocity while increasing stiffness at the whisker base.

METHODS

All procedures involving animals were approved in advance by the Animal Care and Use Committee of Northwestern University.

Data Collection and Data Reduction

The parameters used in the present study are depicted in Fig. 1 and are listed in Table 1.

Data analysis began with the 52 whiskers for which parameters are shown in Table 2. These are the same 52 whiskers of *Reduced Dataset 2* in Table 4 of Belli et al. (2017). Data collection procedures have been described in detail previously (Belli et al. 2017), but, briefly, whiskers were obtained from the left and right arrays of 3 male and female Sprague-Dawley rats (SD, #400; Charles River) with ages between 3 and 13 mo. All whiskers were obtained by cutting the whisker near its base instead of plucking the whisker from the follicle, ensuring that the portion of the whisker internal to the follicle was not included in the mass measurement.

All whiskers were massed using a Mettler Toledo UMX2 microbalance (0.1-μg resolution) within 2–3 h after cutting to prevent dehydration. To test for any possible effects of dehydration, we performed a control experiment in which eight whiskers were massed within 1 h after cutting and then remassed 3, 8, 12, and 15 days later. Whiskers were stored in folded aluminum foil, which were then stored in a plastic freezer bag with a zipper. Results, shown in Table 3, indicate that dehydration did not have a significant effect on the mass of the whisker when we compared the mass 15 days after cutting to the mass 1 h after trimming (2-sided, Wilcoxon signed-rank test, $P < 0.11$). Note that these results are not likely to generalize to all storing conditions in all laboratories.

After massing was performed, the 52 whiskers were scanned on a flatbed scanner at 1,200 dpi (Epson Perfection 4180 Photo) and imaged under a light microscope (Olympus BX60) to obtain measurements of whisker geometry including the medulla. The whisker was cut in 2 at the location where the medulla terminated, and both proximal and distal segments were remassed within 24–48 h and rescanned to estimate the arc length of each segment.

Four whisker segments were lost before they could be massed (indicated as NaNs in Table 2), leaving a total of forty-eight whiskers with complete parameter sets. These forty-eight whiskers were assessed for the presence of extreme outlier values. We searched for outliers in mass, base and tip diameters, arc length, volume, and average density. Extreme outliers were identified as any value more than three standard deviations from the mean.

We found two outlier whiskers for *rat 1*: the B2 whisker was an outlier in proximal average density (10.1 mg/mm^3), and the β-whisker was an outlier in distal average density (17.1 mg/mm^3). The data for these two whiskers are shown in *rows 5* and *18* of Table 2, which are in bold italic and correspond to the same two rows of Table 4 of Belli et al. (2017). These outliers almost certainly occurred due to human error when measuring the geometry of these particular whiskers.

Table 1. *Measured and computed whisker variables*

Measured Variables	
Variable Name	Description
D_{Base}	Diameter of the whisker at its base
D_{Tip}	Diameter of the whisker at its tip
D_{MedT}	Diameter of the whisker at the location where the medulla terminates
D_{Med}	Diameter of the medulla at its base
$D_{Med\_Tip} \equiv 0$	Diameter of the medulla at its tip is defined to be 0
S_{Total}	Total arc length of the whisker
S_{Prox}	Arc length of the whisker proximal to medulla termination
S_{Dist}	Arc length of the whisker distal to medulla termination
M_{Total}	Total mass of the whisker
M_{Prox}	Mass of the whisker proximal to medulla termination
M_{Dist}	Mass of the whisker distal to medulla termination
Calculated Variables	
Variable Name	Description
$R_{Base} \equiv D_{Base}/2$	Radius of the whisker at its base
$R_{Tip} \equiv D_{Tip}/2$	Radius of the whisker at its tip
$R_{MedT} \equiv D_{MedT}/2$	Radius of the whisker at the location where the medulla terminates
$R_{Med} \equiv D_{Med}/2$	Radius of the medulla at its base
$Slope_R \equiv (R_{Base} - R_{Tip})/S_{Total}$	Radius slope
S_{Extend}	Extended length of the proximal whisker (extrapolated length used in the calculation of I_{Mass})
V_{Total}	Volume of the whisker (calculated as truncated cone)
V_{Prox}	Volume of the whisker proximal to medulla termination (calculated as truncated cone)
V_{Dist}	Volume of the whisker distal to medulla termination (calculated as truncated cone)
V_{Med}	Volume of the whisker medulla (calculated as a cone with a tip diameter of 0)
$\rho_{Total} \equiv M_{Total}/V_{Total}$	Average density of the entire whisker
$\rho_{Prox} \equiv M_{Prox}/V_{Prox}$	Average density of the whisker proximal to medulla termination
$\rho_{Dist} \equiv M_{Dist}/V_{Dist}$	Average density of the whisker distal to medulla termination
$\rho \equiv M_{Total}/(V_{Total} - V_{Med})$	Density of the cortex and cuticle of the whisker, excluding the medulla
I_{Area}	Area moment of inertia
I_{Mass}	Mass moment of inertia

Table 2. *Whisker parameters used in the present study*

Rat No.	Sex	Side	Whisker	D_{Base}, μm	D_{Med}, μm	D_{MedT}, μm	D_{Tip}, μm	S_{Total}, mm	S_{Prox}, mm	S_{Dist}, mm	M_{Total}, μg	M_{Prox}, μg	M_{Dist}, μg
1	F	R	A1	139	49	45	5	37.5	25.8	11.7	246.2	229.9	16.3
1	F	R	A2	104	12	45	12	28.7	21.0	7.7	128.3	115.6	12.7
1	F	R	A3	85	14	51	3	19.9	8.5	11.4	60.0	46.6	13.4
1	F	R	B1	160	54	43	6	46.9	32.9	14.0	361.4	348.5	12.9
1	***F***	***R***	***B2***	***73***	***17***	***48***	***5***	***19.6***	***7.7***	***11.9***	***239.7***	***225.9***	***13.8***
1	F	R	C1	163	44	39	4	50.4	38.0	12.4	426.5	417.0	9.5
1	F	R	C2	166	56	43	4	35.2	25.0	10.2	283.1	274.3	8.8
1	F	R	C3	125	33	50	5	23.2	13.2	10.0	120.2	109.6	10.6
1	F	R	C4	100	24	64	3	15.6	6.0	9.6	58.8	44.2	14.6
1	F	R	C6	53	11	49	5	4.2	4.1	0.1	NaN	NaN	NaN
1	F	R	D1	205	71	38	5	56.5	45.9	10.6	NaN	638.1	NaN
1	F	R	D2	178	74	45	7	37.4	27.3	10.1	339.9	329.7	10.2
1	F	R	D4	107	35	58	14	14.4	7.1	7.3	66.9	53.9	13.0
1	F	R	E1	213	84	38	8	49.6	42.4	7.2	634.1	628.3	5.8
1	F	R	E3	174	68	37	9	25.6	19.8	5.8	NaN	216.4	NaN
1	F	R	E4	134	52	52	5	17.0	9.9	7.1	97.1	89.0	8.1
1	F	R	α	145	43	43	6	47.0	31.2	15.8	274.9	261.3	13.6
1	***F***	***R***	***β***	***161***	***45***	***43***	***6***	***40.3***	***38.9***	***1.4***	***424.2***	***410.8***	***13.4***
1	F	R	γ	158	54	43	4	51.0	39.1	11.9	NaN	374.2	NaN
2	M	R	A1	143	44	29	4	43.9	34.9	9.0	292.9	287.3	5.6
2	M	R	A3	95	26	44	3	21.9	12.0	9.9	76.4	67.3	9.1
2	M	R	A4	75	11	55	19	12.0	4.8	7.2	39.0	25.1	13.9
2	M	R	B1	163	60	40	5	52.0	42.3	9.7	466.7	459.1	7.6
2	M	R	B2	148	51	37	7	36.6	28.4	8.2	265.5	260.0	5.5
2	M	R	B3	89	24	47	3	19.2	10.6	8.6	62.0	53.4	8.6
2	M	R	B4	81	10	62	3	13.1	4.3	8.8	40.6	25.8	14.8
2	M	R	C2	159	52	40	4	36.5	28.0	8.5	327.6	320.5	7.1
2	M	R	C3	115	29	38	3	19.9	13.7	6.2	96.3	91.5	4.8
2	M	R	C4	101	16	53	4	15.0	7.6	7.4	63.5	54.1	9.4
2	M	R	D1	203	68	34	4	52.1	45.6	6.5	675.4	671.2	4.2
2	M	R	D5	105	22	60	4	12.9	5.9	7.0	54.9	44.4	10.5
2	M	R	E3	151	58	39	4	26.6	21.0	5.6	207.3	202.6	4.7
2	M	R	E4	132	47	45	4	18.5	12.5	6.0	112.3	106.5	5.8
2	M	R	E5	93	31	55	3	10.9	5.2	5.7	39.0	31.7	7.3
2	M	R	α	154	47	39	4	50.3	40.8	9.5	379.9	372.5	7.4
2	M	R	β	134	40	38	7	45.1	36.3	8.8	251.4	243.7	7.7
2	M	R	γ	134	44	41	4	49.7	41.3	8.4	375.3	368.1	7.2
2	M	R	δ	101	25	41	6	35.8	28.2	7.6	170.8	164.1	6.7
3	M	L	A1	154	60	39	6	41.7	30.3	11.4	277.1	268.9	8.2
3	M	L	A4	76	16	48	5	13.9	6.4	7.5	39.5	32.1	7.4
3	M	L	B1	171	68	40	3	48.2	37.7	10.5	414.2	405.8	8.4
3	M	L	B2	153	50	38	5	35.3	26.1	9.2	239.3	233.7	5.6
3	M	L	B3	99	27	41	5	20.6	12.8	7.8	74.3	68.6	5.7
3	M	L	C2	167	56	40	3	36.6	27.7	8.9	307.9	301.5	6.4
3	M	L	C4	103	26	51	3	16.5	8.9	7.6	71.1	63.1	8.0
3	M	L	D3	134	57	41	6	24.9	18.3	6.6	150.2	145.6	4.6
3	M	L	D4	136	45	46	5	20.6	14.5	6.1	135.9	130.6	5.3
3	M	L	D6	81	18	65	4	8.6	2.9	5.7	23.6	14.3	9.3
3	M	L	E3	158	62	44	5	26.4	20.2	6.2	208.0	202.7	5.3
3	M	L	E6	92	15	59	3	6.4	3.0	3.4	26.0	19.9	6.1
3	M	L	α	160	48	48	3	44.9	37.1	7.8	343.0	334.5	8.5
3	M	L	β	171	53	38	5	54.9	49.6	5.3	477.7	470.7	7.0

Rows in bold italic indicate whiskers that were found to be outliers and removed from analysis (see main text for details). D_{Base}, diameter of the whisker at its base; D_{Med}, diameter of the medulla at its base; D_{MedT}, diameter of the whisker at the location where the medulla terminates; D_{Tip}, diameter of the whisker at its tip; M_{Dist}, mass of the whisker distal to medulla termination; M_{Prox}, mass of the whisker proximal to medulla termination; M_{Total}, total mass of the whisker; S_{Dist}, arc length of the whisker distal to medulla termination; S_{Prox}, arc length of the whisker proximal to medulla termination; S_{Total}, total arc length of the whisker; F, female; L, left; M, male; NaN, not a number; R, right.

Compared with other whiskers with similar total arc lengths, the proximal arc length (S_{Prox}) for the B2 whisker and the distal arc length (S_{Dist}) for the β-whisker were noticeably too short relative to their total arc lengths (S_{Total}). These 2 outlier whiskers were removed from analysis, yielding a final data set of 46 whiskers with no missing observations or outliers.

All figures in the present work use this data set of 46 whiskers. Of the 46 whiskers, 13 were from the right side of a female rat, 19 whiskers were from the right side of a male rat, and 14 whiskers were from the left side of a 2nd male rat. The female rat was ~13 mo old and weighed ~350 g, and both male rats were ~3 mo old and weighed ~300 g.

Mechanical Properties of a Hollow, Tapered Whisker

The goal of the present work was to characterize how the geometric features of a vibrissa influence some of its mechanical properties and thus the signals that will be generated during active tactile sensing. We, therefore, computed several mechanical properties based on the experimentally measured data, including the mass moment of inertia,

Table 3. *Whisker mass did not vary significantly ≤15 days postcutting*

	Whisker Mass, μg				
Whisker Identity	1 h	3 days	8 days	12 days	15 days
A1	127.1	127.5	127.8	126.5	127.5
B1	82.1	82.2	83.3	81.4	82.1
γ	381.7	381.5	380.2	379.2	380.5
C1	327.0	329.3	327.9	329.2	329.2
C3	87.2	86.9	87.1	87.1	86.5
δ	416.0	418.5	417.4	417.3	418.0
D2	105.5	105.6	104.3	104.8	104.6
Unknown	210.9	211.8	211.4	211.2	210.9

the area moment of inertia at the whisker base, and the amount that the whisker deflects under its own weight.

Assumptions about densities of the cuticle, cortex, and medulla. As indicated in Fig. 1, the whisker consists of the cortex, the cuticle, and the medulla. The cortex is densely packed with desiccated hair protein known as keratin. The cuticle is a thin layer of keratin surrounding and protecting the cortex. Recent work on human hair has shown that the cuticle contains β-keratin, whereas the cortex is composed of α-keratin (Stanić et al. 2015), and we expect that a similar difference between cuticle and cortex also holds for rodent vibrissae. However, the present work did not quantify the geometry of the cuticle separately from the cortex, and, therefore, the two materials are assumed to have the same density. The medulla is a porous, weblike structure in the proximal portion of the whisker that is filled with air pockets (Chernova 2003; Hausman 1930). Because the medulla has such a low density, it is often approximated as hollow (Adineh et al. 2015; Voges et al. 2012). We follow the convention of these previous studies in assuming that the medulla has negligible density in all calculations that follow.

Assumptions about proximal and distal slopes. Previous work in both mice (Hires et al. 2016) and rats (Belli et al. 2017) reported that the slope differs between the proximal and distal regions. The difference is indicated in the schematic of Fig. 1 and illustrated in more detail in Fig. 2*A*. In the rat, the proximal radius slope and average distal radius slope are statistically the same when averaged over all whiskers. However, when the ratio of proximal slope to distal slope is analyzed as a function of column, 11/16 whiskers from columns 1 and 2 have proximal slopes greater than distal slopes, whereas only 5/23 whiskers from columns 3–6 and 1/7 whiskers from the Greek arc have proximal slopes greater than distal slopes. These results are confirmed in Fig. 2*B*. We accounted for these differences in radius slope in the calculations that follow.

Note that the present work implicitly assumes a piecewise linear profile for the slope of a rat whisker, with a change point at the location of medulla termination (dividing proximal and distal segments). This choice for change-point location was based on the extremely tight correlation ($r^2 = 0.97$) between medulla length and total whisker length found in Belli et al. (2017). Quantifying nonlinear slope profiles within proximal and distal segments would require a higher-resolution analysis in which radius is measured at many points along the whisker arc length (Hires et al. 2016; Ibrahim and Wright 1975; Williams and Kramer 2010).

Mass moment of inertia as a function of whisker geometry. The mass moment of inertia of the vibrissa (I_{Mass}) measures the resistance of the whisker to rotation. We used the method of superposition to compute the mass moment of inertia for a straight whisker ("superposition approach"; APPENDIX A), and we used a differential disk-integral approach to compute the mass moment of inertia for a whisker with intrinsic curvature (disk-integral approach; APPENDIX B).

Here, we briefly describe the superposition approach because it is used in the first few sections of RESULTS. As derived in APPENDIX A, the mass moment of inertia for a straight whisker is given by:

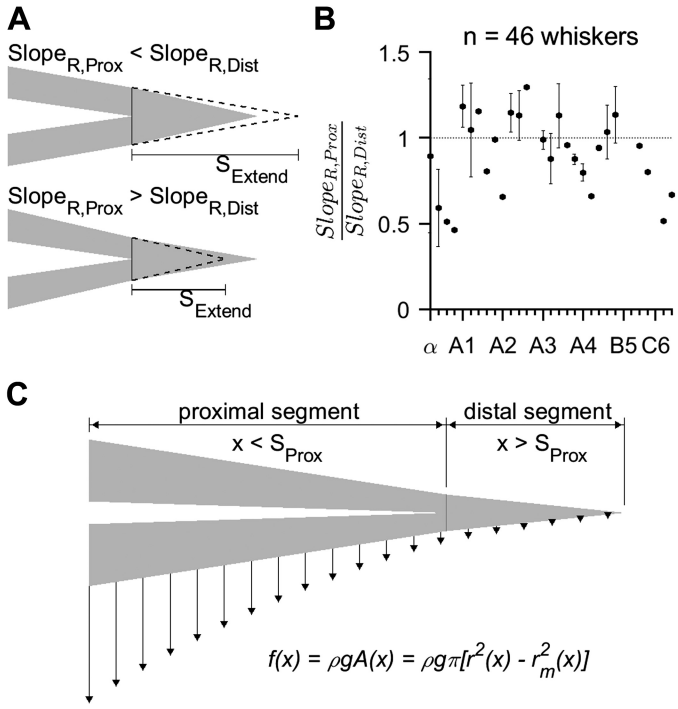

Fig. 2. Computing whisker deflection under its own weight, including the effects of different proximal and distal slopes. *A*: schematic of slope variation. Whisker has a proximal region (Prox) that contains a hollow medulla and a distal region (Dist) that is solid. As illustrated in the schematic (not to scale), previous studies have found that the radius slope ($Slope_R$) differs between the proximal and distal regions. S_{Extend}, extended length of the proximal whisker. *B*: ratio of proximal to distal radius slope. *X*-axis sorts whiskers by column and then by row within each column. *C*: deflection of a tapered whisker with a medulla under its own weight. Schematic is not to scale, and the cuticle is not shown for visual clarity. Outer cross-sectional radius of the whisker (r) and inner cross-sectional radius of the medulla (r_m) are given by *Eqs. 3* and *4*, respectively. We derived a function, $f(x)$, that describes the distributed load of the whisker resulting from its own weight. Black vertical vectors indicate this force per unit length. Vector magnitudes in the distal region decrease quadratically. In the proximal region, the decrease in vector magnitude is approximately quadratic, but it is not exactly, due to the presence of the medulla. ρ, Density of the whisker cortex; $A(x)$, cross-sectional area of whisker cortex as a function of x; g, gravity.

$$I_{Mass} = \frac{1}{60}\pi\{3R_{Base}{}^4S_{Extend} + 2R_{Base}{}^2S_{Extend}{}^3 - 3R_{Med}{}^4S_{Prox} - 2R_{Med}{}^2S_{Prox}{}^3 + 3R_{MedT}{}^4[S_{Dist} - S_{Extend} + S_{Prox}] + 2R_{MedT}{}^2[S_{Dist} - S_{Extend} + S_{Prox}][S_{Dist}{}^2 + S_{Extend}{}^2 + 3S_{Extend}S_{Prox} + 6S_{Prox}{}^2 + S_{Dist}(S_{Extend} + 4S_{Prox})]\}\rho. \quad (1a)$$

In *Eq. 1a*, R_{Base} is the radius at the whisker base, R_{Med} is the radius of the medulla at the whisker base, R_{MedT} is the radius of the whisker at the point of medulla termination, and ρ is the density of the whisker cortex.

The variable S_{Extend} allows us to account for the slope differences between proximal and distal regions. S_{Extend} is the extrapolated full length of the whisker had it retained the slope of its proximal portion for its full length. It is also illustrated in Fig. 2*A*. APPENDIX A explains the mathematical basis for S_{Extend} in further detail.

If the proximal and distal slopes of the whisker were the same, then $S_{Extend} \equiv S_{Prox} + S_{Dist}$, and *Eq. 1a* simplifies to the following expression:

$$I_{Mass} = \frac{1}{60}\pi(-3R_{Med}{}^4S_{Prox} - 2R_{Med}{}^2S_{Prox}{}^3 + 3R_{Base}{}^4S_{Total} + 2R_{Base}{}^2S_{Total}{}^3). \quad (1b)$$

It is worth emphasizing that in *Eqs. 1a* and *1b*, and throughout this entire study, the density ρ without a subscript denotes the material density of keratin that forms the whisker excluding the medulla. In other words, ρ represents the combined density of the cortex and cuticle. Later portions of this study will employ the variables ρ_{Total}, ρ_{Prox}, and ρ_{Dist}, which represent densities averaged over select regions of the whisker as defined in Table 1.

Area moment of inertia at the whisker base. The stiffness at the whisker base is given by the product of the cross-sectional area moment of inertia (I_{Area}) and Young's modulus (E). For a given value of Young's modulus, a larger area moment of inertia means that the whisker is more resistant to bending. Given the presence of the medulla at the whisker base, I_{Area} can be described as (Hibbeler 2014):

$$I_{\mathrm{Area}} = \frac{\pi}{4}\left({R_{\mathrm{Base}}}^4 - {R_{\mathrm{Med}}}^4\right). \tag{2}$$

Vertical deflection of the whisker under the influence of gravity reflects a trade-off between whisker mass and stiffness. Like any cantilever beam, the mass of a whisker will cause it to deflect vertically ("droop") under the influence of gravity. The magnitude of vertical deflection reflects a trade-off between the mass of the whisker and its stiffness. The deflection curve of the whisker is denoted by $\mathrm{v}(x)$: it describes the vertical deflection at every position x along the whisker length. To derive the deflection curve, we first obtained an analytical expression for its second-order derivative. This equation was then numerically integrated twice to obtain $\mathrm{v}(x)$. Here, we provide the derivation of the second-order derivative of the deflection curve.

Consistent with previous studies (Birdwell et al. 2007; Hires et al. 2013), we modeled the whisker as a straight, tapered cantilever beam. Although whiskers have intrinsic curvature (Ahissar and Knutsen 2008; Quist and Hartmann 2012; Towal et al. 2011), the principle of superposition allows us to add the amount of deflection to the amount of intrinsic curvature. Superposition is valid because the radius of curvature of the whisker is more than five times the maximum diameter of the whisker (Hibbeler 2014).

A schematic illustrating the distributed load involved in computing the deflection curve is shown in Fig. 2*C*. The cross-sectional radius of the whisker cortex (r) and inner radius occupied by the medulla (r_{m}) were written as functions of the distance (x) from the whisker base:

$$r(x) = \begin{cases} \dfrac{R_{\mathrm{MedT}} - R_{\mathrm{Base}}}{S_{\mathrm{Prox}}}x + R_{\mathrm{Base}}, x \le S_{\mathrm{Prox}} \\ \dfrac{R_{\mathrm{Tip}} - R_{\mathrm{MedT}}}{S_{\mathrm{Dist}}}\left(x - S_{\mathrm{Prox}}\right) + R_{\mathrm{MedT}}, x \ge S_{\mathrm{Prox}} \end{cases} \tag{3}$$

$$r_{\mathrm{m}}(x) = \frac{-R_{\mathrm{Med}}}{S_{\mathrm{Prox}}}x + R_{\mathrm{Med}}. \tag{4}$$

To provide intuition for *Eqs. 3* and 4, we reiterate (see Table 1) that R_{MedT} is different from R_{Med}. R_{Med} is the base radius of the medulla. R_{MedT} is the outer radius of the whisker at the location where the medulla terminates.

With the development of expressions for the radius of the whisker and the radius of the medulla as functions of the longitudinal distance from whisker base, x, it follows that the cross-sectional area of the whisker cortex as a function of x, $A(x)$, is given by:

$$A(x) = \pi\left[r(x)^2 - r_{\mathrm{m}}(x)^2\right]. \tag{5}$$

Next, at each position (x) along its length, the whisker experiences a distributed load (f) due to its own weight (Fig. 2*C*). The distributed load has dimensions of force per unit length. The expression for the distributed load was obtained by finding the weight of keratin in an infinitesimal cross-section of the whisker. This weight is the product of the density of keratin (ρ), the acceleration due to gravity (g), and the cross-sectional area (A) occupied by keratin at each position (x):

$$f(x) = \rho g A(x) = \rho g \pi\left[r(x)^2 - r_{\mathrm{m}}(x)^2\right]. \tag{6}$$

Given the expression for the distributed load, standard elastic beam bending equations can be used to compute the shear force and bending moment as functions of x (Hibbeler 2014). Specifically, the integral of the distributed load over the length of any segment of a beam yields the shear force, $\mathrm{F}(x)$. The integral of shear force over the length of any segment of a beam yields bending moment $\mathrm{M}(x)$:

$$F(x) = \int f(x)\mathrm{d}x \tag{7}$$

$$\mathrm{M}(x) = \int F(x)\mathrm{d}x = \int\int f(x)\mathrm{d}x\mathrm{d}x. \tag{8}$$

For a thin beam, the moment $\mathrm{M}(x)$ is related to the curvature $\kappa(x)$ of the whisker by:

$$\kappa(x) = \frac{\mathrm{M}(x)}{EI(x)}. \tag{9}$$

For small angles, the curvature is the second derivative of the deflection curve:

$$\mathrm{v}''(x) = \kappa(x). \tag{10}$$

so that:

$$\mathrm{v}''(x) = \frac{\mathrm{M}(x)}{EI(x)}. \tag{11}$$

It is important to note that I is a function of x, and it depends on the medulla:

$$I(x) = \frac{1}{4}\pi\left[r(x)^4 - r_{\mathrm{m}}(x)^4\right]. \tag{12}$$

Note that $I(x)$ refers to the area moment of inertia at each location (x) along the length of the whisker. In contrast, I_{Area} (as defined in *Eq. 2*) specifically refers to the area moment of inertia at the base of each whisker. In other words, I_{Area} is identical to $I(x)$ evaluated at the base of the whisker: $I_{\mathrm{Area}} \equiv I(x)|_{x=0}$.

Substituting the bending moment (*Eq. 8*) and area moment of inertia (*Eq. 12*) into *Eq. 11* yields two second-order differential equations for $\mathrm{v}''(x)$. One equation is for the proximal region of the whisker, $\mathrm{v}_{\mathrm{Prox}}(x)$, and the second equation is for the distal region, $\mathrm{v}_{\mathrm{Dist}}(x)$.

We performed these substitutions using Wolfram Mathematica and found that for the proximal segment of the whisker ($x \le S_{\mathrm{Prox}}$) the second-order derivative of the deflection curve $\mathrm{v}_{\mathrm{Prox}}(x)$ is given by:

$$\mathrm{v}_{\mathrm{Prox}}''(x) = \frac{4\rho g S_{\mathrm{Prox}}\left\{-\dfrac{{R_{\mathrm{Med}}}^2\left[S_{\mathrm{Prox}} - x\right]^4}{4{S_{\mathrm{Prox}}}^3} + \dfrac{S_{\mathrm{Prox}}\left[R_{\mathrm{Base}} + \dfrac{\left(R_{\mathrm{MedT}} - R_{\mathrm{Base}}\right)x}{S_{\mathrm{Prox}}}\right]^4}{4\left[R_{\mathrm{MedT}} - R_{\mathrm{Base}}\right]^2}\right\}}{3E\left\{\left[R_{\mathrm{Base}} + \dfrac{\left(R_{\mathrm{MedT}} - R_{\mathrm{Base}}\right)x}{S_{\mathrm{Prox}}}\right]^4 - \left[R_{\mathrm{Med}} - \dfrac{R_{\mathrm{Med}}x}{S_{\mathrm{Prox}}}\right]^4\right\}}. \tag{13a}$$

For the proximal segment, we assumed a clamped boundary condition at the whisker base (Bagdasarian et al. 2013) so that both the displacement and the slope of the whisker are 0 at the base, i.e.:

$$\mathrm{v}_{\mathrm{Prox}}(0) = 0; \mathrm{v}_{\mathrm{Prox}}'(0) = 0. \tag{13b}$$

The second equation, also found using Mathematica, describes the distal portion of the whisker, where $x \ge S_{\mathrm{Prox}}$, and is given by:

$$\mathrm{v}_{\mathrm{Dist}}''(x) = \frac{\rho g {S_{\mathrm{Dist}}}^2}{3E\left(R_{\mathrm{Tip}} - R_{\mathrm{MedT}}\right)^2}. \tag{14a}$$

Two compatibility conditions were applied to solve for v_{Dist} because the displacement and slope at the termination point of the medulla ($x = S_{Prox}$) must be identical for both proximal and distal regions of the whisker:

$$v_{Dist}(S_{Prox}) = v_{Prox}(S_{Prox}); v'_{Dist}(S_{Prox}) = v'_{Prox}(S_{Prox}). \quad (14b)$$

Notice that this derivation shows that the curvature (i.e., the second-order derivative of the deflection curve) of the distal portion of the whisker is independent of the position x.

When integrated twice, *Eqs. 13a* and *14a* yield the deflection curve $v(x)$ at every point along the whisker length. *Equations 13b* and *14b* give the constants of integration. Although, in theory, *Eqs. 13a* and *14a* could have been integrated analytically, these integrations were quite complicated; it was found easier to compute the integrals numerically using ode45 in MATLAB.

Tip deflection (δ) is defined as the distance that the tip of the whisker is vertically displaced from its original position due to the weight of the whisker. The value of the tip deflection is found by evaluating the deflection curve at the location $x = S_{Total}$.

RESULTS

Importance of Mechanical Properties to the Study of Rat Whiskers

The material properties and mass distribution of a whisker govern its mechanical properties, which dictate both its quasi-static bending and dynamic response. In this first section of RESULTS, we describe how seven variables of interest relate to whisking behavior. We specifically consider the center of mass, mass moment of inertia, radius of gyration, area moment of inertia, and tip deflection as well as two nondimensionalized variables: the normalized radius of gyration and the ratio of tip deflection to arc length.

Variables with dimensions. First, the center of mass (CoM) of a whisker is a point in space for which location is determined by the distribution of mass along the length of the whisker. It is the theoretical point at which all of the distributed mass should be placed to retain the same response to an external force. In theory, if an external force acted on the whisker at its center of mass, the whisker would translate only in the direction of the applied force and would not rotate. The CoM has dimensions of length.

Second, the mass moment of inertia of a whisker (I_{Mass}) directly determines *1*) the torque required to generate a given angular acceleration and *2*) the kinetic energy required to rotate at a given angular velocity. Both angular acceleration and angular velocity are important when describing noncontact whisking (i.e., the rotation in free air of the whisker). From an energy perspective, a low value of the mass moment of inertia is preferred, as it will reduce the kinetic energy and torque required for a given angular velocity and acceleration. I_{Mass} has the unit of mass times length squared and is only defined with respect to a particular axis of rotation.

In conditions such as noncontact whisking, when the whisker can be approximated as a rigid body (Knutsen et al. 2008; O'Connor et al. 2013; Quist et al. 2014), the product of I_{Mass} and the angular acceleration α of the whisker yields the torque (τ) required to rotate the whisker: $\tau = I_{Mass}\alpha$. In addition, again assuming a rigid body approximation, the product of I_{Mass} and the square of the rotational velocity ω yields the kinetic energy (KE) required to rotate the whisker: $KE = (1/2)I_{Mass}\omega^2$. The superposition approach for I_{Mass} is provided in METHODS assuming a straight whisker. The disk-integral approach, accounting for the intrinsic curvature of the whisker, is provided in APPENDIX B for all three Cartesian axes of rotation. All axes are defined with respect to the shape of the whisker and pass through the whisker base (see APPENDIX B).

Third, the radius of gyration of a whisker (R_g) can be thought of in some ways as the rotational analog of the center of mass. Mathematically, the radius of gyration is equal to the square root of (I_{Mass} divided by mass), and it has dimensions of length. The radius of gyration is the theoretical point where all of the distributed mass should be placed to retain the same rotational response to an external torque.

Unlike the CoM, which represents a specific point relative to a chosen origin, the radius of gyration is a scalar. R_g is a distance from a chosen axis of rotation but has no directionality or absolute position in space. In the present study, the axis of rotation always passes through the base of the whisker.

Fourth, the area moment of inertia at the whisker base (I_{Area}) is directly related to the stiffness of the whisker and, therefore, characterizes how much the whisker will bend in response to an imposed moment. For a given imposed moment, a whisker with greater bending stiffness will deflect less than one with smaller bending stiffness. As described in METHODS, the stiffness is the product of the Young's modulus (E) and I_{Area} of the beam. Because the cross-sectional geometry of a whisker varies monotonically (and nearly linearly) from base to tip, the I_{Area} at the base is representative of the entire whisker.

Fifth, the deflection of a whisker under its own weight describes the vertical displacement of each node of the whisker under the influence of gravity. The tip deflection δ is the largest deflection for each whisker, which always takes place at its tip. From a behavioral standpoint, reducing tip deflection will increase the horizontal "reach" of the whisker.

Dimensionless variables. Sixth, the normalized radius of gyration (R_{gN}) effectively describes a trade-off between the arc length of a whisker and its radius of gyration. Both quantities have dimensions of length, so the ratio is nondimensional (R_g/S_{Total}).

Particular to the present study, the normalized radius of gyration is important because whiskers have high aspect ratios (arc length to base diameter), such that the radius of gyration is primarily determined by the arc length. As a result, and as will be further detailed in *Variations in Mechanical Parameters Across the Vibrissal Array*, if whiskers were all perfect, linearly tapering cones with zero tip diameter, they would all have the exact same value of normalized radius of gyration. In other words, the normalized radius of gyration is how much the whisker deviates from a perfect cone. Whiskers are not perfect cones because of the presence of the medulla and the slightly nonlinear slopes (Hires et al. 2016).

Seventh and finally, the deflection-to-length ratio (δ/S_{Total}) is calculated by dividing the tip deflection by the arc length of the whisker. This ratio reflects trade-offs in the rat's sensing volume compared with the energy required for whisking. Increased tip deflection decreases the sensing volume. Theoretically, tip deflections can be reduced either by shortening the whisker or by increasing base diameter (which will increase mass). Thus δ/S_{Total} directly assesses the extent to which each whisker in the array trades off increases in mass to attain an increase in sensing volume.

Density Varies Along the Whisker Length

Both the cuticle and the near-hollow medulla contribute to a nonuniform distribution of keratin material throughout the whisker (Fig. 1). To quantify the variability in mass distribution along the whisker length, we calculated the average density of both the proximal and distal portions of the whisker (Fig. 3*A*). These densities are the variables ρ_{Prox} and ρ_{Dist} in Table 1. As expected, the average density is significantly higher in the distal region than in the proximal region (paired, 2-sided Wilcoxon signed-rank test, $P < 0.001$). The average proximal density is 1.26 mg/mm^3 (SD 0.16 mg/mm^3) with a median of 1.23 mg/mm^3, and the average distal density is 1.69 mg/mm^3 (SD 0.31 mg/mm^3) with a median of 1.62 mg/mm^3.

For comparison, the average density for the entire whisker is 1.28 mg/mm^3 (SD 0.16 mg/mm^3) with a median of 1.26 mg/mm^3. The average density for the entire whisker was computed assuming the whisker volume as the sum of the proximal and distal volumes, thereby accounting for the slight difference in radius slope observed between the proximal and distal regions of the whisker in Fig. 6*A* in Belli et al. (2017).

Two factors are likely to contribute to the difference between proximal and distal densities shown in Fig. 3*A*. First, the presence of the medulla will decrease the average density in the proximal region. Second, the area fraction (and hence the volume fraction) of the whisker occupied by the cuticle increases substantially from proximal to distal (Quist et al. 2011). The cuticle occupies up to 60% of the most distal regions of the whisker (Quist et al. 2011). Given that the cuticle is likely to be of a material (β-keratin) different from the cortex (α-keratin; Stanić et al. 2015), it seems likely that the cuticle contributes significantly to density variations along the whisker length.

To disambiguate the contributions of these two factors, we computed the material density (ρ) of the entire whisker and compared it with the density of the distal region. By definition (Table 1), ρ is computed after subtracting out the volume of the medulla. In other words, ρ is the density of the cortex and cuticle only. The material density was found to be 1.36 mg/mm^3 (SD 0.13 mg/mm^3) with a median of 1.38 mg/mm^3.

When the material density is plotted versus the proximal density (Fig. 3*B*), all points lie just barely above the identity line, indicating that the effect of the medulla is small (paired, 2-sided Wilcoxon signed-rank test, $P < 0.001$). Comparing Fig. 3*B* with Fig. 3*A* further shows that the material density is typically smaller than the distal density, confirming that the presence of the medulla has only a limited effect on the density of the entire whisker. Thus the changes in density along the whisker length can be attributed primarily to the change in volume fraction occupied by the cuticle.

Although the average whisker density is considerably greater in the whisker distal region than in the proximal portion, this nonuniformity has very little effect on the center of mass of the whisker. This result is shown in Fig. 3*C*, which compares the center of mass computed using the material density with that computed using different average densities for the proximal and distal regions of the whisker. When averaged across all 46 whiskers, the center of mass shifted only 2.106% closer to the distal end of the whisker than if the average density had been uniform (paired, 2-sided Wilcoxon signed-rank test, $P < 0.001$). Note that this analysis holds equally well for curved whiskers as for straight whiskers: straight whiskers can be thought of as a special case of curved whiskers with 0 curvature. In other words, the center of mass will change significantly with whisker curvature. However, for a whisker of a given curvature, density variations will have very little effect on the center of mass.

If a whisker were a perfectly straight, uniformly dense cone with tip diameter equal to 0, then by definition its center of mass would always lie at a distance $d = S_{Total}/4$. We computed the center of mass as a fraction of whisker arc length for all 46 whiskers of the data set, assuming the whiskers were straight, and results are shown in Fig. 3*D*. As expected, the center of mass of the whiskers scatters about the value 0.25 [interquartile range (IQR) = 0.0215]. The scatter results from 4 factors: the presence of the medulla, differences in density between cuticle and cortex, differences in slope between proximal and distal regions, and non-0 tip radius.

Mechanical Advantages Conferred by the Medulla

Recall from the mechanical descriptions provided at the beginning of RESULTS that reducing the mass moment of inertia (I_{Mass}) of the whisker would decrease energy expenditure, but increasing the area moment of inertia (I_{Area}) of the whisker would increase stiffness at the base, potentially improving signal transmission. We, therefore, hypothesized that the hollow medulla strikes a balance between decreasing the mass moment of inertia and increasing the area moment of inertia at the whisker base.

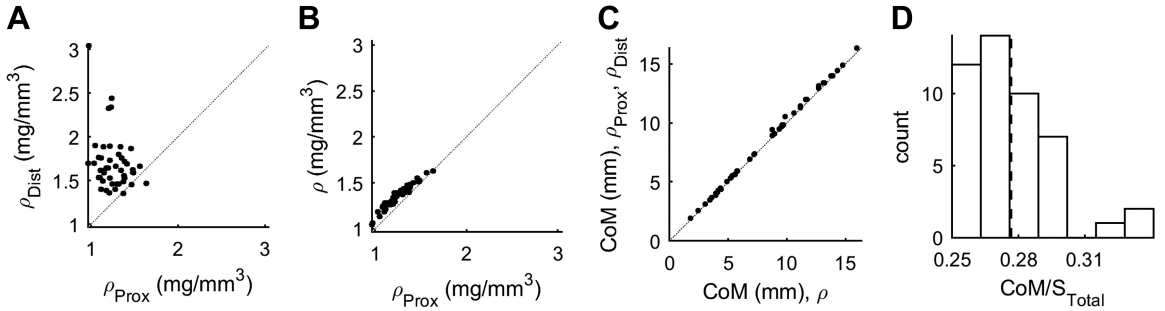

Fig. 3. Variability between proximal and distal densities and its effect on the center of mass of the whisker. *A*: average density of the distal portion of the whisker (ρ_{Dist}) is greater than the average density of the proximal portion (ρ_{Prox}). *B*: material density (ρ) is the density of the cortex and cuticle only and is only slightly greater than ρ_{Prox}. When compared with *A*, it is clear that the medulla is not the primary factor that explains why ρ_{Dist} is greater than ρ_{Prox}. *C*: because of differences in the density distribution, the center of mass (CoM) of the whisker is, on average, ~2.1% more distal than it would have been if the mass had been uniformly distributed. Curvature is neglected in this analysis but would not change these results. *D*: as expected, the center of mass as a fraction of whisker length is close to the theoretical value for a perfect cone, 0.25. Mean (0.277) is marked by a thick, dashed line. S_{Total}, total whisker arc length.

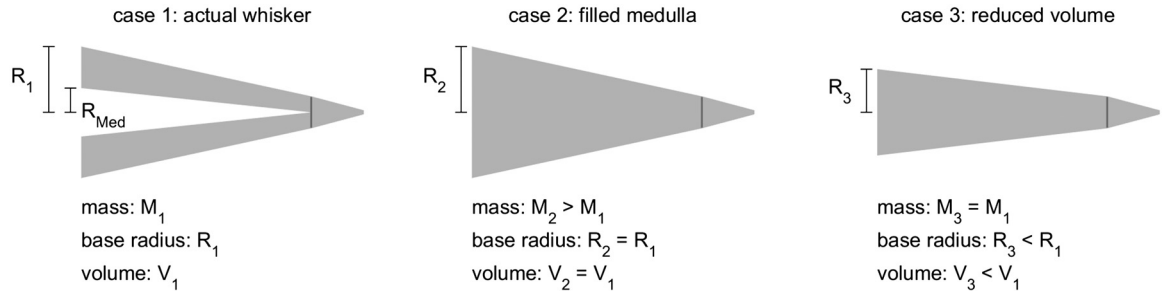

Fig. 4. Comparison of actual whisker morphology to 2 alternative hypothetical geometries. *Case 1* illustrates the actual whisker geometry. *Case 2* has the same outer dimensions as *case 1* but greater mass because the hollow medulla is now assumed to be solid keratin. *Case 3* has the same mass as *case 1*, but the hollow medulla is "squashed" in the proximal region of the whisker. This compression reduces the proximal taper and the base diameter. For visual simplicity, the cuticle is not illustrated in any of the schematics. R_{Med}, radius of the medulla at its base.

To investigate the potential mechanical advantages of the medulla, we compared the actual whisker geometry with two hypothetical whisker geometries, shown in Fig. 4. The "filled medulla" case assumes that the space occupied by the medulla is filled with keratin, just like the whisker cortex. In this scenario, the mass of the whisker increases, but the outer dimensions of the whisker remain constant.

The "reduced volume" case assumes that the total amount of keratin of the whisker remains the same but is distributed closer to the central axis of the whisker. Intuitively, this case corresponds to "squashing" the medulla by bringing the sides of the whisker toward the central axis. In this scenario, the mass of the whisker stays constant, but its volume decreases, and its geometry changes. The new base radius, R_3, is given by the expression:

$$R_3 = \frac{1}{2}\left[\sqrt{(2R_{Base} + R_{MedT})^2 - 4{R_{Med}}^2} - R_{MedT}\right]. \quad (15)$$

Notice that for both the filled medulla and reduced volume cases, only the proximal portion of the whisker is affected; the geometry of the distal portion remains unchanged.

For each of the three cases shown in Fig. 4, we quantified four material and mechanical properties across all whiskers of the array: the whisker mass (M), the area moment of inertia at the base (I_{Area}), the deflection of the tip under the whisker's own weight (δ), and the mass moment of inertia (I_{Mass}) about the axis that passes through the whisker base, orthogonal to the long axis of the whisker. This axis is the primary axis of rotation of the whisker during whisking behavior, so I_{Mass} is directly related to the torque and rotational kinetic energy required for whisking. The I_{Mass} calculation here assumes that whiskers have zero tip diameter, no intrinsic curvature, and that their proximal and distal regions have two distinct slopes.

To generalize the results of this analysis across the entire array, we used the equations of Belli et al. (2017) to determine the geometric parameters for each whisker based only on its row and column identity. These equations are listed in Table 4. Whiskers B5, C6, D6, and E6 were excluded from this analysis because their arc lengths were <10 mm and, therefore, violated the assumptions required to use these equations. For each of the remaining 27 whiskers, the quantities M, I_{Mass}, I_{Area}, and δ were calculated using the material density of the whisker found experimentally ($\rho = 1.36$ mg/mm^3; Fig. 3*B*).

The mean and standard deviation for M, I_{Mass}, I_{Area}, and δ were computed over these 27 whiskers for the three cases shown in Fig. 4. Results are shown in Table 5. Each row of Table 5 lists the percentage difference in these parameters for hypothetical *cases 2* and *3* relative to *case 1* (the actual whisker geometry). This analysis answers questions such as, "When averaged across all whiskers in the array, by how much would I_{Mass} increase if the whiskers were entirely solid?"

For *case 2*, the first row of Table 5 immediately indicates that filling the medulla with keratin (*case 2*) would increase the mass of the whisker on average by $>5\%$ compared with a hollow medulla (*case 1*). This increase in mass also necessarily increases I_{Mass} for *case 2* compared with *case 1*, which would increase the amount of kinetic energy required to rotate the whisker. For *case 3*, the rows for M and I_{Mass} in Table 5 show a slightly less intuitive result: although the mass of the whisker is identical between the reduced volume whisker (*case 3*) and the actual whisker, the mass moment of inertia (I_{Mass}) of *case 3* is slightly smaller than I_{Mass} for the actual whisker. This effect occurs because in *case 3* the mass is redistributed to be closer to the whisker base. In theory, then, *case 3* would decrease the rotational kinetic energy needed for whisking. This effect is very small, however ($<1\%$), and its benefit is likely outweighed by the negative consequences for stiffness described next.

The area moment of inertia at the whisker base (3rd row of Table 5) is important because, along with Young's modulus, it determines the bending stiffness of the whisker at the base. If the base of the whisker is stiff, the same forces and moments will produce a smaller amount of deflection (curvature change). This difference in signal strength will affect the mechanical sensing resolution of the whisker. The geometry of the filled medulla whisker (*case 2*) results in an

Table 4. *Equations used to compute the geometry of all whiskers in the array*

Variable	Equation
Arc length (S_{Total})	$43 + 1.8$ Row $- 7.6$ Col, $S_{Total} > 10$ mm
Proximal arc length (S_{Prox})	$0.95\ S_{Total} - 7.3$
Base diameter (D_{Base})	$0.041 + 0.0020\ S_{Total} + 0.011$ Row $-$ 0.0039 Col
Radius slope (Slope$_R$)	$0.0012 + 0.00017$ Row $- 0.000066$ Col $+$ 0.00011 Col^2
Medulla diameter (D_{Med})	$0.44\ D_{Base} - 0.019$
Tip diameter (D_{Tip})	Calculated from S_{Total}, D_{Base}, and Slope$_R$ ($D_{Tip} \equiv 0$ if $D_{Tip} < 0$)
Medulla termination diameter (D_{MedT})	Calculated from S_{Total}, S_{Prox}, D_{Base}, and Slope$_R$

Col, column.

Table 5. *Effect of the medulla on the mechanical properties of the whisker*

Parameter	Unit	"Filled Medulla" (*Case 2*) Relative to Actual Whisker (*Case 1*)	"Reduced Volume" (*Case 3*) Relative to Actual Whisker (*Case 1*)
Mass (M)	mg	↑ 5.67% (SD 2.66) (worse)	No change
Mass moment of inertia (I_{Mass})	mg·mm^2	↑ 2.75% (SD 1.81) (worse)	***↓ 0.69% (SD 0.35) (better)***
Area moment of inertia at the base (I_{Area})	mm^4	***↑ 0.69% (SD 0.37) (better)***	↓ 12.4% (SD 4.17) (worse)
Tip deflection (δ)	mm	↑ 1.47% (SD 1.05) (worse)	↑ 11.7% (SD 4.21) (worse)

Four mechanical parameters are computed assuming the two hypothetical geometries shown in Fig. 4 and compared with the same parameters computed using the actual whisker geometry. The average and standard deviation of the values across all 27 whiskers are shown for each quantity. Relative to the actual whisker, the filled medulla (*case 2*) undesirably increases I_{Mass} and the amount of tip deflection under the whisker's own weight (δ) while increasing stiffness at the base (I_{Area}) by <1%. The reduced volume results in a slightly lower I_{Mass} (bold italic) but at the cost of significantly decreasing I_{Area} and increasing δ. The assessments "worse" and "better" are based on energy considerations for mass and mass moment of inertia, based on stiffness considerations for area moment of inertia, and based on considerations of sensing volume for tip deflection. Cells in bold italic indicate parameters that were better for the hypothetical whisker geometry rather than the actual whisker.

area moment of inertia only slightly bigger than that of the actual whisker (*case 1*). The reduced volume whisker (*case 3*), on the other hand, has an area moment of inertia substantially smaller than that of the actual whisker (*case 1*). These results make excellent intuitive sense because, by definition, area moment of inertia is proportional to the fourth power of the radius.

Finally, the last row of Table 5 illustrates that both the filled medulla whisker (*case 2*) and the reduced volume whisker (*case 3*) increase tip defection relative to the actual whisker geometry (*case 1*). Of the parameters discussed so far, tip deflection most clearly exposes the trade-off between two quantities for which desired values have opposite trends: it is desirable to reduce mass (and thus I_{Mass}) to reduce the energy required for whisking, whereas it is desirable for I_{Area} to be large to resist bending, preventing the whisker from "drooping," and to increase the mechanical signals at the whisker base in response to a given deformation. Comparing the magnitude of tip deflection across the three cases thus suggests that the actual whisker geometry (*case 1*) is superior to the alternative proposed geometries.

In summary, the hollow medulla strikes a balance between decreasing I_{Mass} and increasing I_{Area} at the whisker base. Although the actual geometry achieves only the second-highest bending stiffness (compare with *case 2*), it decreases M, I_{Mass}, and δ. Similarly, the actual whisker geometry has a slightly higher I_{Mass} than *case 3*, but this disadvantage is outweighed by the much larger increase in stiffness and decrease in tip deflection.

On Average, the Intrinsic Curvature of the Whisker has a Larger Influence on I_{Mass} than Does Variation in Whisker Slope

Real rodent whiskers are characterized by two important geometric features: curvature (Knutsen et al. 2008; Towal et al. 2011) and nonlinear slope (Hires et al. 2016). However, the analysis of the previous section, including Table 5, uses the method of superposition to calculate I_{Mass}, which neglects intrinsic curvature (see APPENDIX A). The calculation of APPENDIX A assumes a straight whisker with two distinct slopes in proximal and distal regions. Therefore, as shown in APPENDIX B, we developed a second, disk-integral approach to compute I_{Mass}. This approach accounts for intrinsic curvature and neglects slope differences. The two approaches (superposition and disk-integral) converge for the case of a straight, single-sloped whisker: the error between the two approaches is <0.0012% (see APPENDIX B).

To summarize, the superposition approach accounts for slope variations but not intrinsic curvature, whereas the disk-integral approach accounts for intrinsic curvature but not slope variations. Accounting for both slope variation and curvature simultaneously would require a purely numerical approach, which lies outside the scope of the present work. We used the two approaches to evaluate how each of the two geometric features, slope and curvature, affected I_{Mass}. The I_{Mass} of whiskers with a straight, single-slope geometry calculated using the disk-integral approach was used as the baseline standard for comparison.

The change of I_{Mass} from baseline to a 2-slope geometry (while maintaining 0 curvature) is shown in Fig. 5*A*. Accounting for 2 slopes causes I_{Mass} to increase for most but not all whiskers. The reason for this variability is that the radius slope could either decrease or increase from proximal to distal, depending on the individual whisker in the experimental data. For those whiskers for which distal slope is steeper than the proximal slope, accounting for 2 slopes "removes" material from the whisker and thus decreases I_{Mass}. In contrast, for those whiskers for which proximal slope is steeper than the distal slope, accounting for 2 slopes "adds" material from the whisker and thus increases I_{Mass}.

The change in I_{Mass} from baseline to a curved geometry (while maintaining a single slope) is shown in Fig. 5*B*. Accounting for curvature resulted in a decrease in I_{Mass} for all whiskers, without exception. This decrease is expected because I_{Mass} is directly related to the distance of the mass distribution of the whisker from its axis of rotation. Because the intrinsic curvature of the whisker causes it to curve toward its primary axis of rotation (at the whisker base), the value of I_{Mass} necessarily decreases as curvature increases.

Comparing the average and standard deviation of the data plotted in black (calculated based on average curvature and slope variation) in each data set, it is evident that curvature has a much larger effect on I_{Mass} [−40.77% (SD 13.19%)] than two slopes [8.37% (SD 16.72%)].

Variations in Mechanical Parameters Across the Vibrissal Array

The overall goal of the present work was to develop mechanical models that could be used to simulate the signals across the entire whisker array during active whisking behav-

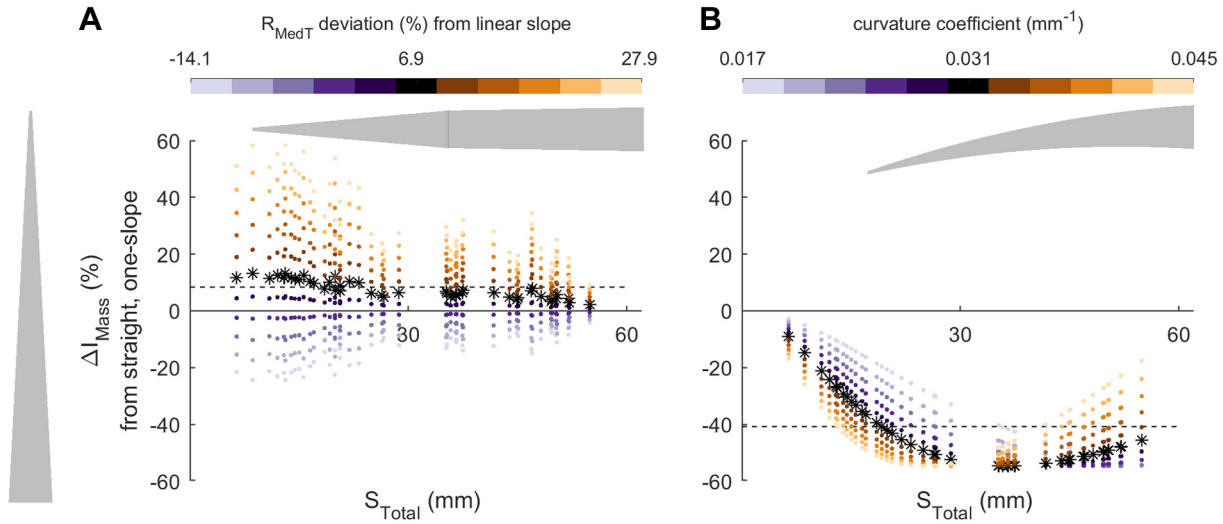

Fig. 5. Effects of curvature and slope variation on the mass moment of inertia (I_{Mass}) of the whisker. *A*: this subplot shows how I_{Mass} changes when a whisker with no intrinsic curvature is assumed to have 2 different slopes as opposed to a single slope. Changes in I_{Mass} are plotted as a function of the total arc length (S_{Total}). At each value of S_{Total}, the black asterisk indicates the I_{Mass} change assuming the average deviation of radius of the whisker at medulla termination point (R_{MedT}) from [base radius (R_{Base}) minus tip radius (R_{Tip})]/S_{Total} across all of the whiskers (6.9%). Different colored data points at that same value of S_{Total} then indicate the change in I_{Mass} assuming the slope difference indicated by the color. Range of values tested (−14.1 to 27.9%) represent the mean plus and minus the standard deviation [6.9% (SD 21.0%)] of slope differences computed from Table 2. Dashed, horizontal line shows the mean of all data points. *B*: this subplot shows how I_{Mass} changes as the intrinsic curvature of a whisker increases. Whisker is assumed to have a single slope, computed as (R_{Base} minus R_{Tip})/S_{Total} for each whisker from Table 2. At each value of S_{Total}, the black asterisk indicates the change in I_{Mass} assuming the average curvature (0.031/mm) across all whiskers [average curvature computed from data in Belli et al. (2017)]. Each colored dot at that same value of S_{Total} indicates the change in I_{Mass} assuming the curvature indicated by the color. Dashed, horizontal line shows the mean of all data points.

ior. We, therefore, examined each of the mechanical parameters in Table 4 (M, I_{Mass}, I_{Area}, and δ) as a function of location within the vibrissal array. To provide intuition for the effect of density variations, we also computed the volume of each whisker; this plot can be visually compared with the mass.

Results are shown in Fig. 6*A*, which compares values computed from experimental data with values computed using the equations shown in Table 4 assuming a constant cortex density of 1.36 mg/mm^3. As in the analysis of Table 5, 4 of the 31 whiskers (B5, C6, D6, and E6) were excluded from the equa-

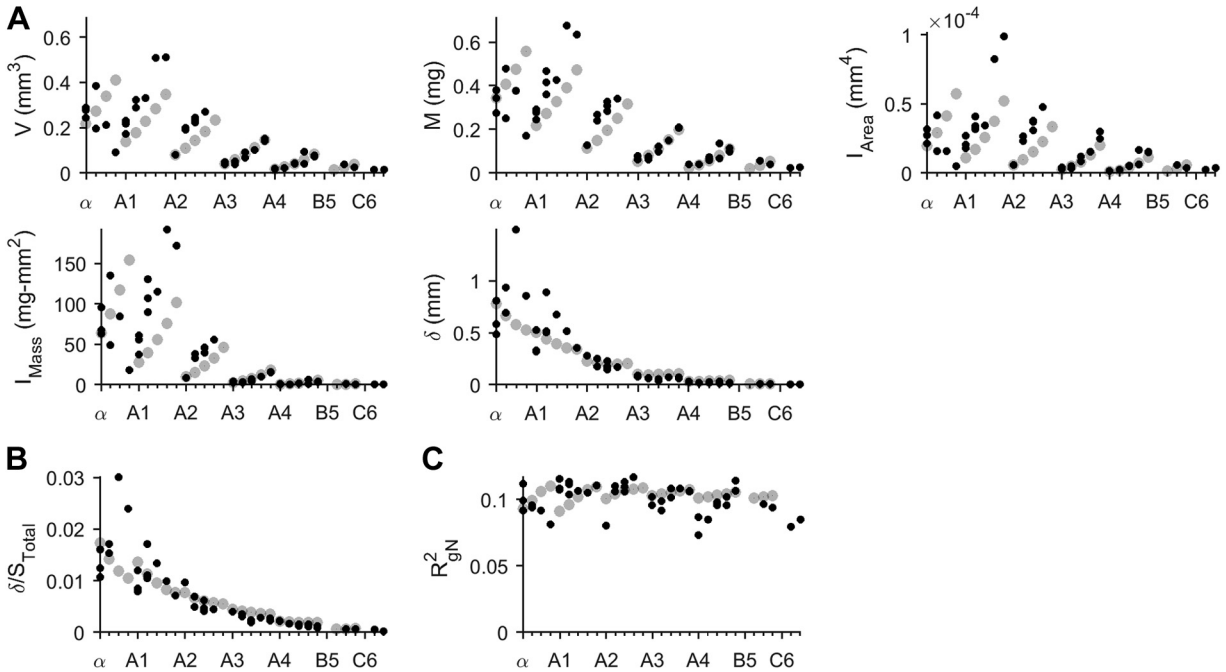

Fig. 6. Mechanical and material properties as a function of whisker identity. Black circles show experimental data from all 46 whiskers in the data set. Gray circles are trends computed from the equations in Table 4 for 27 whiskers. *A*: volume (V), mass (M), area moment of inertia (I_{Area}), mass moment of inertia (I_{Mass}), and tip defection (δ) of the whisker all decrease as a function of column position. In accordance with the analysis of Fig. 5, the calculation for I_{Mass} accounting for the intrinsic curvature of whiskers neglects the difference between proximal and distal slopes. *B*: dimensionless "deflection-to-length ratio" (δ/S_{Total}) decreases as a function of column position. More rostral whiskers have the smallest tip deflection for a given whisker length. Longer, more caudal whiskers droop significantly more under their own weight, even when normalized by whisker length. *C*: normalized square of the radius of gyration (R_{gN}^2) is essentially 0.1 for all whiskers.

tion-based calculation, so only 27 equation-based data points are shown. The most obvious trend in the figure is that all 5 variables tend to decrease as a function of column position. This result is expected because the whiskers tend to become smaller from caudal to rostral (i.e., from column 1 to column 6). A more subtle effect is that within each column, all parameters except for δ tend to increase slightly from the A row to the E row (ventral to dorsal).

It is also interesting to examine how several dimensionless parameters scale across the array. Two of the four variables listed in Table 4, tip deflection (δ) and the mass moment of inertia (I_{Mass}), can be combined with the arc length of the whisker and whisker mass to form physically informative dimensionless parameters.

The tip deflection (δ) can be divided by the total arc length (S_{Total}) to form the dimensionless parameter δ/S_{Total}, i.e., the deflection-to-length ratio, as shown in Fig. 6*B*. As its name suggests, this quantity represents how far a whisker of a given length will deflect at its tip under the influence of gravity. This dimensionless parameter reveals that the smallest whiskers have the smallest tip deflection for a given whisker length. The larger, more caudal whiskers are likely to extend the rat's sensory volume (Hobbs et al. 2015; Huet and Hartmann 2014) but deflect more under their own weight, even after normalizing for arc length.

The second important dimensionless parameter is related to the mass moment of inertia. Dividing I_{Mass} by the whisker mass M yields the square of the radius of gyration ($R_g^2 \equiv I_{Mass}/M$). When normalized by the square of the whisker length, we obtain the normalized square of the radius of gyration [$R_{gN}^2 \equiv I_{Mass}/(MS_{Total}^2)$], as shown in Fig. 6*C*.

For a solid cone with tip diameter equal to zero, base radius r, and height h, it can be shown that the square of the radius of gyration is $R_g^2 = (1/20)(2h^2 + 3r^2)$ (*Eq. A9* in APPENDIX A), and the normalized square of the radius of gyration can then be calculated:

$$R_{gN}^2 = \frac{1}{20}\left(2 + 3\frac{r^2}{h^2}\right). \quad (16)$$

If $r \ll h$, as is the case for all rodent macrovibrissae, then R_{gN}^2 is always approximately, although not exactly, 0.1 (IQR = 0.0155 for data in black and IQR = 0.055 for data in gray in Fig. 6). In other words, R_{gN}^2 characterizes how far the whisker shape deviates from a perfect cone.

DISCUSSION

Civil engineers use I-beams, C-beams, and other "hollow-structured sections" to construct bridges and buildings. The design of these structural elements is based on elastic beam bending theory: material is distributed far from the neutral axis to increase resistance to bending without increasing weight (Hibbeler 2014). With its hollow medulla, the rat whisker exhibits similar mechanical advantages. In addition, systematic variations in the "droop-to-length" ratio across the array lend support to the idea (Ahl 1986; Brecht et al. 1997; Carvell and Simons 1990; Hobbs et al. 2015, 2016; Thé et al. 2013; Wineski 1983) that whiskers in different row and column positions have been precisely tuned to diversify the tactile signals received.

Advantages of the Whisker Morphology over Hypothetical Alternatives

Previous studies, which divided the whisker into quartiles, found that the medulla occupied between 50 and 75% of the whisker length (Adineh et al. 2015; Voges et al. 2012). More recent work (Belli et al. 2017) has quantified medulla length with ~0.1-mm resolution. Figure 4, *A–D*, of that work demonstrates close linear relationships between the dimensions of the medulla and those of the entire whisker. The fraction of the volume occupied by the medulla of the whisker is smaller for shorter whiskers than for longer whiskers, so rostral whiskers will tend to have a more uniform average density than caudal whiskers. These density variations will be important for accurate dynamic simulations, for example, in analyses of noncontact whisking, interactions with textured surfaces, and during collisions (Boubenec et al. 2012; Hires et al. 2013; Kan et al. 2013; Khatri et al. 2010; Quist et al. 2014).

Consistent with the presence of the medulla, Fig. 3*A* of the present work confirms that the proximal region of the whisker has a lower average density than the more distal region. An important caveat, however, is that the medulla is not a large contributing factor to the average density variations observed in Fig. 3*A*. A more important factor seems to be that the cuticle occupies an increasing volume fraction of the whisker toward its distal regions (Quist et al. 2011). Given that the cuticle probably has a density different from the cortex (Stanić et al. 2015), these material differences could account for much of the observed density variation.

The presence of the medulla within the whisker offers several key advantages over the two hypothetical geometries shown in Fig. 4 and described in Table 4. Most obviously, the medulla decreases the total mass of the whisker compared with a solid (filled) whisker. In addition, the medulla reduces the amount that the whisker deflects under its own weight. Table 4 shows that without the presence of the medulla, tip deflection increases by ~1.5% for the filled whisker and by over ~12% in the reduced volume case. However, even though the medulla is proportionally larger in caudal whiskers, the deflection-to-length ratio is not constant across the array. Most caudal whiskers deflect more under their own weight in proportion to their length (Fig. 6*B*). The maximum deflection of any whisker under the influence of gravity is ~1 mm.

Finally, as shown in Table 4, the medulla serves to increase stiffness at the whisker base (I_{Area}) while reducing the amount of energy required to whisk at a given rotational velocity (I_{Mass}). If the medulla were filled, I_{Area} would increase, but only by <1%, and this improvement would come at the cost of increasing mass by ~5.7% and mass moment of inertia by ~2.8%. If the whisker volume were reduced (the "squashed" whisker), I_{Mass} would decrease slightly (by <1%), but the trade-off would be a large decrease in stiffness at the whisker base (by >12%).

Although these changes may seem small, a 3–12% change for all whiskers across the array will have a significant effect, especially given that a rat whisks continuously between 5 and 25 Hz during long durations of active tactile exploration (Berg and Kleinfeld 2003; Welker 1964).

Center of Mass and Radius of Gyration

Regardless of curvature, the variability in density along the length of the whisker has only a small effect on the center of mass or radius of gyration of the whisker. About 2.1% difference was observed when the center of mass was computed assuming a constant density for the whisker instead of variable proximal/distal density.

The radius of gyration, R_g, is the point at which all of the mass of an object should be placed to maintain a rotational inertia equivalent to that of the original object. The radius of gyration can be thought of as the rotational analog to the center of mass. An important difference, however, is that the center of mass does not depend on the direction in which the object is translated. In contrast, the radius of gyration depends on the axis of rotation. In the present work, R_g was computed about the axis of rotation associated with natural whisking behavior and assuming that the whisker does have intrinsic curvature.

For a solid cone, the square of R_g depends on the sum of the length squared and the radius squared (*Eq. 16*). Because the whisker is so long and thin, the contribution of the radius is negligible, so *Eq. 16* simplifies to ${R_g}^2 = 0.1S^2$. Thus, if the whisker were a perfect solid cone, its radius of gyration would always be at a location 31.6% of the whisker length.

Figure 6*C* clearly shows that the whiskers deviate at most ~10% from perfect cones, shifting the value of $(R_g/S_{Total})^2$ from 0.100 to a maximum of 0.110 and a minimum of 0.091 for equation-based whiskers. Thus the radius of gyration for a typical whisker will always be found at distances that range from ~30.1 to ~33.2% of the whisker length. Even if the whisker is damaged, R_g will scale with whisker length and mass, so the rat does not have to learn a new dynamic scaling law. This invariance is a result of the high length-to-radius aspect ratio.

From a motor control standpoint, these results imply that the muscle torque required to rotate the whisker at a given angular acceleration will always be proportional to the mass of the whisker multiplied by a constant fraction (~0.11) of the square of the whisker length. Assuming that muscle force is linear with the number of fibers (Oatis 2004), if the number of muscle fibers per motor unit for each whisker scaled with MS_{Total}^2, then the motor system could send the same rate of spikes to each intrinsic muscle and all whiskers would rotate with the same angular acceleration. Alternatively, the number of neurons in the facial motor nucleus activated by a presynaptic neuron (e.g., a neuron in M1) could scale with MS_{Total}^2 to achieve the same effect. Note, however, that this analysis neglects the mass and drag of the follicle itself as well as the viscoelastic properties of the tissue.

Summary and Future Work

The present study has quantified several important parameters that are essential for accurate simulations of whisker dynamics. We anticipate that future simulation studies will exploit these results to quantify the mechanosensory signals associated with vibrissotactile exploratory behavior; these signals can then be correlated with neural activity (Bush et al. 2016a).

In addition, increasing evidence points to the idea that different groups of whiskers may be best suited for different functions (Ahl 1986; Brecht et al. 1997; Carvell and Simons 1990; Hobbs et al. 2015, 2016; Thé et al. 2013; Wineski 1983). These groupings may correspond, at least in part, to muscle groups that activate different regions of whiskers (Haidarliu et al. 2010, 2011, 2012, 2013, 2017; Hill et al. 2008; Simony et al. 2010). The varying geometric and motor relationships across the array will diversify the signals acquired during active tactile sensation. An important area of future work will be to examine the effect of geometry on both whisker dynamics and quasistatic bending from external forces and moments (Hires et al. 2013; Huet and Hartmann 2016; Kaneko et al. 1998; Solomon and Hartmann 2008).

On a more speculative note, we observe that, although not quantified in the present work, three locations appear to converge along the length of each whisker: the location where the medulla terminates (Belli et al. 2017), the location of the change point at which the cuticle thickness increases significantly (Quist et al. 2011), and the location at which whiskers tend to curve out of the plane (Knutsen et al. 2008; Towal et al. 2011). It would be interesting if these three locations were, in fact, the same.

APPENDIX A: METHOD OF SUPERPOSITION TO COMPUTE THE MASS MOMENT OF INERTIA OF A WHISKER

Here, we show the computation for I_{Mass} assuming a straight, tapered cone with zero tip diameter, two slopes, and a hollow proximal region. This approach was used in the analyses of Table 5 and Figs. 4 and 5*A*.

Overview of the Calculation

Computing I_{Mass} for the three cases shown in Fig. 4 requires three steps.

Step 1. We first derive the general expression for I_{Mass} of a cone rotating about the vertical axis at its base as well as the general expression for I_{Mass} of a cone rotating about a vertical axis at a distance L from its base (Fig. A1*A*). The cone here and in the rest of the appendix is assumed to have negligible tip diameter.

Step 2. With these two general expressions, we then compute I_{Mass} for the four imaginary whisker sections shown in Fig. A1*B*. *Section 1* is a cone that represents the outer shape of the whisker, extrapolated as if the proximal taper continued all the way until the radius vanishes to 0. This imaginary whisker section has an extended arc length, S_{Extend}:

$$S_{Extend} = \frac{R_{Base}\, S_{Prox}}{R_{Base} - R_{MedT}}. \quad (A1)$$

Section 2 is a cone the same shape as the distal portion of the extended whisker of *section 1*. *Section 3* is a cone the same shape as the medulla. Finally, *section 4* represents the distal geometry of the real whisker.

Note that the geometry for *case 3* of Fig. 4 must be computed differently, because we have squashed the whisker, so we end up with an equivalent radius, R_{Eqv}, and an equivalent extended arc length, S_{Extend_Eqv}:

$$R_{Eqv} = \frac{1}{2}\left[-R_{MedT} + \sqrt{-4{R_{Med}}^2 + \left(2R_{Base} + R_{MedT}\right)^2}\right] \quad (A2)$$

$$S_{Extend\_Eqv} = \frac{R_{Base}\, S_{Prox}}{R_{Eqv} - R_{MedT}}. \quad (A3)$$

Step 3. With these imaginary whisker sections defined in Fig. A1*B*, we can see that *cases 1–3* are composed of the following sections:

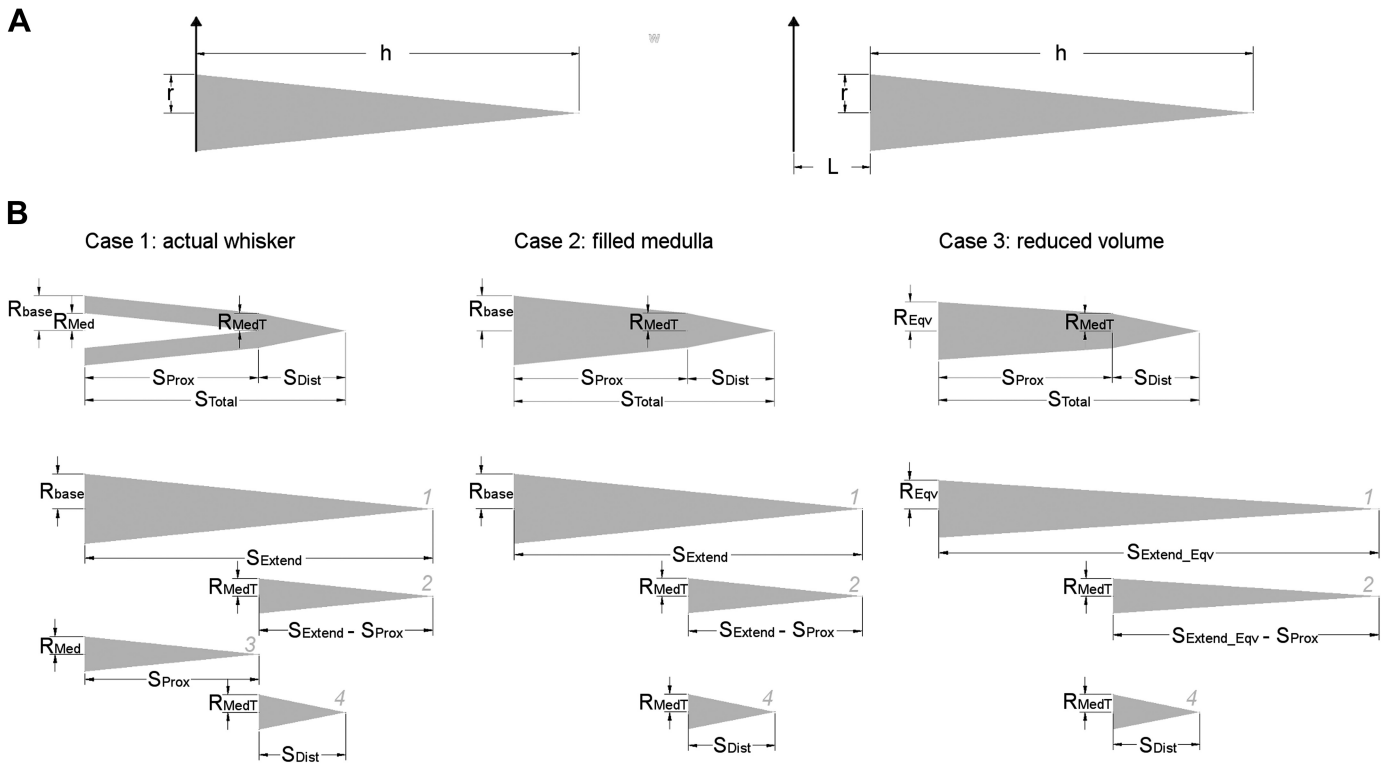

Fig. A1. Calculation of mass moment of inertia using superposition. *A*: *left* shows a schematic of a cone of radius r and length h rotating about its vertical axis at the base. *Right* shows a cone of radius r and length h rotating about its vertical axis at a distance L from the base. In both panels, the axis of rotation is shown as a thick arrow. *B*: schematics show the geometry of the actual whisker (*case 1*) along with the hypothetical cases of a "filled medulla" (*case 2*) and "reduced volume" (*case 3*). Each case is shown with its corresponding imaginary whisker sections (1–4) that are combined using superposition to determine the mass moment of inertia. R_{base}, base radius; R_{Eqv}, equivalent radius; R_{Med}, radius of the medulla at its base; R_{MedT}, radius of the whisker at medulla termination point; S_{Dist}, distal arc length; S_{Extend}, extended arc length; S_{Prox}, proximal arc length; S_{Total}, total arc length.

$$I_{Case1} = I_1 - I_2 - I_3 + I_4 \tag{A4}$$

$$I_{Case2} = I_1 - I_2 + I_4 \tag{A5}$$

$$I_{Case3} = I_{1eqv} - I_{2eqv} + I_4. \tag{A6}$$

General Expression for I_{Mass} of a Cone Rotating About the Vertical Axis at its Base and Rotating About the Vertical Axis at a Distance L from its Base

According to Hibbeler (2014), the mass moment of inertia of a cone (mass m, base radius r, and height h) rotating about the vertical axis that passes through its tip is:

$$I_{m,\text{tip}} = \frac{3}{5}m\left(\frac{r^2}{4} + h^2\right). \tag{A7}$$

The center of mass (CoM) of a cone is $(3/4)h$ from its tip. Applying the parallel axis theorem and thereby offsetting the axis of rotation back to the CoM, we obtain:

$$I_{m,\text{CoM}} = I_{m,\text{tip}} - m\left(\frac{3h}{4}\right)^2 = \frac{3}{5}m\left(\frac{r^2}{4} + h^2\right) - \frac{9}{16}mh^2 = \frac{3}{80}m\left(h^2 + 4r^2\right). \tag{A8}$$

Applying the parallel axis theorem a second time, we obtain the mass moment of inertia of a cone rotating about the vertical axis that goes through its base:

$$I_{m,\text{base}} = I_{m,\text{CoM}} + m\left(\frac{h}{4}\right)^2 = \frac{3}{80}mh^2 + \frac{3}{20}mr^2 + \frac{1}{16}mh^2 = \frac{1}{20}m\left(2h^2 + 3r^2\right). \tag{A9}$$

To calculate the mass moment of inertia about an axis at a distance L from the base of the cone:

$$I_{m,L\text{fromB}} = I_{m,\text{CoM}} + m\left(\frac{h}{4} + L\right)^2 = \left(\frac{h}{4} + L\right)^2 m + \frac{3}{80}m\left(h^2 + 4r^2\right). \tag{A10}$$

When written in terms of the density, ρ, the mass of a cone is, by definition:

$$m = \frac{1}{3}\pi r^2 h\rho. \tag{A11}$$

We can thus rewrite *Eqs. A8–A10* in terms of the density:

$$I_{m,\text{CoM}} = \frac{1}{80}h\pi r^2\left(h^2 + 4r^2\right)\rho \tag{A12}$$

$$I_{m,\text{base}} = \frac{1}{60}h\pi r^2\left(2h^2 + 3r^2\right)\rho \tag{A13}$$

$$I_{m,L\text{fromB}} = \frac{1}{60}h\pi r^2\left(2h^2 + 10hL + 20L^2 + 3r^2\right)\rho. \tag{A14}$$

Calculating I_{Mass} for the Four Imaginary Whisker Sections

We now calculate I_{Mass} for each of the four sections shown in Fig. A1*B*. All variables used in the equations that follow are illustrated in Fig. A1*B* and are identical to the variables used in the main text.

For each of the four sections, we simply insert the appropriate dimensions (see Fig. A1*A*) into the general expressions represented by *Eqs. A12–A14*:

$$I_1 = I_{m,\mathrm{base}} = \frac{1}{60} S_{\mathrm{Extend}} \pi {R_{\mathrm{Base}}}^2 \left(2{S_{\mathrm{Extend}}}^2 + 3{R_{\mathrm{Base}}}^2\right)\rho \quad (A15)$$

$$I_2 = I_{m,L\mathrm{fromB}} = \frac{1}{60}\left(S_{\mathrm{Extend}} - S_{\mathrm{Prox}}\right)\pi {R_{\mathrm{MedT}}}^2\left[2\left(S_{\mathrm{Extend}} - S_{\mathrm{Prox}}\right)^2 + 10\left(S_{\mathrm{Extend}} - S_{\mathrm{Prox}}\right)S_{\mathrm{Prox}} + 20{S_{\mathrm{Prox}}}^2 + 3{R_{\mathrm{MedT}}}^2\right]\rho \quad (A16)$$

$$I_3 = I_{m,\mathrm{base}} = \frac{1}{60} S_{\mathrm{Prox}} \pi {R_{\mathrm{Med}}}^2 \left(2{S_{\mathrm{Prox}}}^2 + 3{R_{\mathrm{Med}}}^2\right)\rho \quad (A17)$$

$$I_4 = I_{m,L\mathrm{fromB}} = \frac{1}{60} S_{\mathrm{Dist}} \pi {R_{\mathrm{MedT}}}^2 \left(2{S_{\mathrm{Dist}}}^2 + 10 S_{\mathrm{Dist}} S_{\mathrm{Prox}} + 20{S_{\mathrm{Prox}}}^2 + 3{R_{\mathrm{MedT}}}^2\right)\rho. \quad (A18)$$

For *case 3*, however, we must use $S_{\mathrm{Extend\_Eqv}}$ and R_{Eqv} in *Eqs. A13* and *A14*:

$$I_{1\mathrm{eqv}} = \frac{1}{60} S_{\mathrm{Extend\_Eqv}} \pi {R_{\mathrm{Eqv}}}^2 \left(2{S_{\mathrm{Extend\_Eqv}}}^2 + 3{R_{\mathrm{Eqv}}}^2\right)\rho \quad (A19)$$

$$I_{2\mathrm{eqv}} = \frac{1}{60}\left(S_{\mathrm{Extend\_Eqv}} - S_{\mathrm{Prox}}\right)\pi {R_{\mathrm{MedT}}}^2\left[2\left(S_{\mathrm{Extend\_Eqv}} - S_{\mathrm{Prox}}\right)^2 + 10\left(S_{\mathrm{Extend\_Eqv}} - S_{\mathrm{Prox}}\right)S_{\mathrm{Prox}} + 20{S_{\mathrm{Prox}}}^2 + 3{R_{\mathrm{MedT}}}^2\right]\rho. \quad (A20)$$

Superposition of I_{Mass} of the Four Imaginary Whisker Sections to Compute I_{Mass} for Each of the Three Cases Shown in Fig. 4

We can now write the complete mass moment of inertia equations described in the overview of the calculations (*Eqs. A4–A6*) and seen in Fig. A1*B* for each of the three cases in Fig. 4. In all three cases, we have computed I_{Mass} about the vertical axis that passes through the whisker base.

Case 1: actual whisker morphology with a medulla.

$$I_{Case1} = \frac{1}{60}\pi\left\{3{R_{\mathrm{Base}}}^4 S_{\mathrm{Extend}} + 2{R_{\mathrm{Base}}}^2 {S_{\mathrm{Extend}}}^3 - 3{R_{\mathrm{Med}}}^4 S_{\mathrm{Prox}} - 2{R_{\mathrm{Med}}}^2 {S_{\mathrm{Prox}}}^3 + 3{R_{\mathrm{MedT}}}^4\left[S_{\mathrm{Dist}} - S_{\mathrm{Extend}} + S_{\mathrm{Prox}}\right] + 2{R_{\mathrm{MedT}}}^2\left[S_{\mathrm{Dist}} - S_{\mathrm{Extend}} + S_{\mathrm{Prox}}\right]\left[{S_{\mathrm{Dist}}}^2 + {S_{\mathrm{Extend}}}^2 + 3S_{\mathrm{Extend}}S_{\mathrm{Prox}} + 6{S_{\mathrm{Prox}}}^2 + S_{\mathrm{Dist}}\left(S_{\mathrm{Extend}} + 4S_{\mathrm{Prox}}\right)\right]\right\}\rho \quad (A21)$$

Case 2: filled medulla.

$$I_{Case2} = \frac{1}{60}\pi\left\{3{R_{\mathrm{Base}}}^4 S_{\mathrm{Extend}} + 2{R_{\mathrm{Base}}}^2 {S_{\mathrm{Extend}}}^3 + 3{R_{\mathrm{MedT}}}^4\left[S_{\mathrm{Dist}} - S_{\mathrm{Extend}} + S_{\mathrm{Prox}}\right] + 2{R_{\mathrm{MedT}}}^2\left[S_{\mathrm{Dist}} - S_{\mathrm{Extend}} + S_{\mathrm{Prox}}\right]\left[{S_{\mathrm{Dist}}}^2 + {S_{\mathrm{Extend}}}^2 + 3S_{\mathrm{Extend}}S_{\mathrm{Prox}} + 6{S_{\mathrm{Prox}}}^2 + S_{\mathrm{Dist}}\left(S_{\mathrm{Extend}} + 4S_{\mathrm{Prox}}\right)\right]\right\}\rho \quad (A22)$$

Case 3: reduced volume (squashed whisker).

$$I_{Case3} = \frac{1}{60}\pi\left\{3{R_{\mathrm{Eqv}}}^4 S_{\mathrm{Extend\_Eqv}} + 2{R_{\mathrm{Eqv}}}^2 {S_{\mathrm{Extend\_Eqv}}}^3 + 3{R_{\mathrm{MedT}}}^4\left[S_{\mathrm{Dist}} - S_{\mathrm{Extend\_Eqv}} + S_{\mathrm{Prox}}\right] + 2{R_{\mathrm{MedT}}}^2\left[S_{\mathrm{Dist}} - S_{\mathrm{Extend\_Eqv}} + S_{\mathrm{Prox}}\right]\left[{S_{\mathrm{Dist}}}^2 + {S_{\mathrm{Extend\_Eqv}}}^2 + S_{\mathrm{Extend\_Eqv}}S_{\mathrm{Prox}} + 6{S_{\mathrm{Prox}}}^2 + S_{\mathrm{Dist}}\left(S_{\mathrm{Extend\_Eqv}} + 4S_{\mathrm{Prox}}\right)\right]\right\}\rho \quad (A23)$$

APPENDIX B: METHOD OF DIFFERENTIAL DISK INTEGRATION TO COMPUTE THE MASS MOMENT OF INERTIA OF A WHISKER

Here, we show the calculation for I_{Mass} about all three Cartesian axes, assuming that the whisker is a curved, tapered cone with zero tip diameter and a single slope. This approach was used in the analyses of Figs. 5*B* and 6. At the end of this appendix, we also demonstrate that solutions from the approaches shown in APPENDIX A and APPENDIX B converge to within numerical error for the special case of a straight whisker with a single slope.

Assumptions of the Calculation

The whisker is assumed to be a tapered cone with zero tip diameter, a single linear taper (slope), and an intrinsic curvature that places the whisker concave downward along the z_0-axis, as shown in Fig. B1. The whisker is assumed to be planar, so there is no curvature in the third dimension (x_0–y_0 plane). The curvature along the longitudinal midline is parametrized by a second-order equation, where the coefficient of curvature, A, is constant:

$$z_0(x) = -Ax_0^2. \quad (B1)$$

If the whisker were straight, I_{Mass} about the y_0 and z_0 axes would be the same, but the inclusion of intrinsic curvature requires us to calculate I_{Mass} about all three axes: x_0, y_0, and z_0.

Dividing the Whisker into Differential Disks and Calculating I_{Mass} of Each

The integral is formulated by dividing the cone into infinitely many differential disks and integrating along the x_0-axis as defined in Fig. B1. The disks are "tilted" because of the intrinsic curvature of the whisker.

Because the whisker tapers, the radii of the disks, r, vary with arc length. At an arbitrary point along the whisker length, the area of each disk is πr^2 and the unit mass per unit length is $\rho\pi r^2$, where ρ represents the whisker density. The distances from the centroid of each disk to the three axes of rotation of the whisker are z, $\sqrt{x^2+z^2}$, and x, respectively. We also define the angle α (see Fig. B1*A*) based on the normal to the local slope of the whisker and the x_0-axis. Along the curve defined by *Eq. B1*, α can be expressed as a function of x as in *Eq. B2*:

$$\alpha(x) = \tan^{-1}\left(-\frac{1}{\mathrm{slope}}\right) = \tan^{-1}\left[-\frac{1}{z'(x)}\right] = \tan^{-1}\left(-\frac{1}{-2Ax}\right) = \tan^{-1}\left(\frac{1}{2Ax}\right). \quad (B2)$$

In *Eq. B2*, the coefficient A represents the intrinsic curvature of the whisker, just as in *Eq. B1*.

To formulate the integral for each disk then requires three steps. First, we define z' (see Fig. B1*B*) to formulate a double integral over the variables y and z', which correspond to the two major axes along the plane where the disk lies. Note that z' is tilted at an angle ($\pi/2 - \alpha$) from the z-axis. Also note that r varies with location along the arc

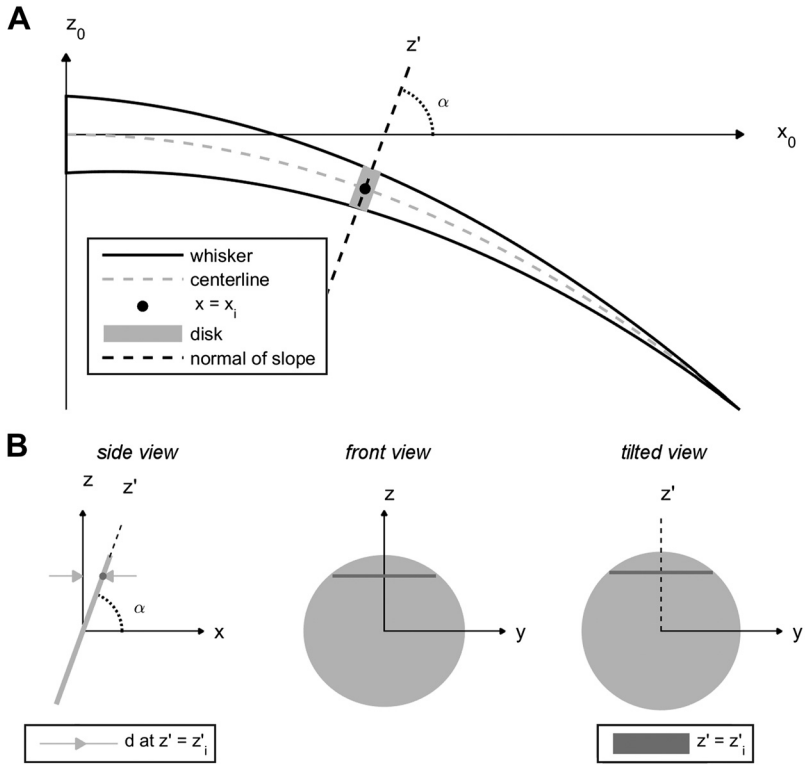

Fig. B1. Calculation of mass moment of inertia for a curved whisker. *A*: idealized shape of a curved, tapered whisker is shown with black solid lines. Curvature of the centerline of the whisker (gray dashed line) is described by a 2nd-order polynomial equation, and the whisker is imagined to rotate about a vertical axis (z_0) passing through its base. Whisker is divided into differential disk-shaped cross-sections. There is 1 disk (shaded light gray) with infinitesimal thickness at each point (black dot) along the whisker arc length. Direction normal to the slope (black dashed line) and the angle (α) at which the normal line is tilted from the *x*-axis are also shown. *B*: 3 alternative views of the gray cross-sectional disk in *A* are provided. Mass moment of inertia of the disk is calculated by an area integral over the *y*-*z*′ plane. In all 3 of the figures, the integrand of the area integral at any *z*′-location is an infinitesimally thin horizontal bar shown in dark gray. In the leftmost figure, the horizontal bar is seen in the side view, so it appears only as a dark gray dot. For rotation about the z_0-axis, the distance *d* from a given location along the *z*′-axis to the vertical axis (*z*-axis) is also shown as the distance between light gray arrows. Center figure and rightmost figure both show "front-on" views of the cross-sectional disk in *A*, but the center figure is an ellipse because it shows the view in the *y*-*z* plane, whereas the rightmost figure is a circle because it shows the view in the *y*-*z*′ plane.

length but is independent of *y* and *z*′. On the *y*-*z*′ plane, the circle that defines the boundary of the disk can be expressed as $y^2 + z'^2 = r^2$. Therefore, the upper and lower limits for one of the two variables, *y*, are $\sqrt{r^2-z'^2}$ and $-\sqrt{r^2-z'^2}$, respectively.

Second, when a disk tilted at an angle, $\alpha(x)$, is divided into infinitesimal horizontal bars parallel to the *y*-axis, the shortest distance, *d*, of each bar from the axes of rotation, *x*-, *y*-, and *z*-axes, are $z'\sin[\alpha(x)]$, z', and $z'\cos[\alpha(x)]$, respectively.

With the two expressions above, we can now formulate and solve double integrals to acquire I_{Mass} of each disk about all three axes of rotation, as shown in *Eqs. B3a*, *-b*, and *-c*:

$$I_{\text{disk},x} = \int d^2dm = \rho \int d^2dA = \rho \int \left(z'\sin\alpha\right)^2 dydz'$$
$$= \rho\int_{-r}^{r}\int_{-\sqrt{r^2-z'^2}}^{\sqrt{r^2-z'^2}} z'^2\sin\alpha^2\, dydz' = \rho\int_{-r}^{r} z'^2\sin\alpha^2\left(2\sqrt{r^2-z'^2}\right)dz'$$
$$= \left\{\frac{1}{4}\rho\sin\alpha^2\left[z'\sqrt{r^2-z'^2}\left(-r^2+2z'^2\right) + r^4\tan^{-1}\frac{z'}{\sqrt{r^2-z'^2}}\right]\right\}_{-r}^{r}$$
$$= \frac{1}{4}\rho\pi r^4\sin\alpha^2 = \frac{1}{4}\rho\pi r^4\sin\left(\tan^{-1}\frac{1}{2Ax}\right)^2 \qquad (B3a)$$

$$I_{\text{disk},y} = \rho\int\left(z'\right)^2 dydz' = \rho\int_{-r}^{r}\int_{-\sqrt{r^2-z'^2}}^{\sqrt{r^2-z'^2}} z'^2\, dydz' = \frac{1}{4}\rho\pi r^4 \qquad (B3b)$$

$$I_{\text{disk},z} = \rho\int\left(z'\cos\alpha\right)^2 dydz' = \rho\int_{-r}^{r}\int_{-\sqrt{r^2-z'^2}}^{\sqrt{r^2-z'^2}} z'^2\cos\alpha^2\, dydz'$$
$$= \frac{1}{4}\rho\pi r^4\cos\alpha^2 = \frac{1}{4}\rho\pi r^4\cos\left(\tan^{-1}\frac{1}{2Ax}\right)^2. \qquad (B3c)$$

Last but not least, for each disk, we apply the parallel axis theorem to calculate the mass moment of inertia at a distance from the axis of rotation passing through the whisker base, as described in *Eqs. B4a*, *-b*, and *-c*. Recall that the mass of the disk is $\rho\pi r^2$, and the parallel distances of the centroid of the disk from the three axes of rotation are *z*, $\sqrt{x^2+z^2}$, and *x*, respectively.

$$I_{\text{Disk}_d,x} = I_{\text{disk},x} + m_{\text{disk}}d^2 = \frac{1}{4}\rho\pi r^4\sin\left(\tan^{-1}\frac{1}{2Ax}\right)^2 + \rho\pi r^2 z^2$$
$$= \rho\pi r^2\left[\frac{1}{4}r^2\sin\left(\tan^{-1}\frac{1}{2Ax}\right)^2 + A^2x^4\right] \qquad (B4a)$$

$$I_{\text{Disk}_d,y} = I_{\text{disk},y} + m_{\text{disk}}d^2 = \frac{1}{4}\rho\pi r^4 + \rho\pi r^2\left(x^2+z^2\right)$$
$$= \rho\pi r^2\left\{\frac{r^2}{4} + x^2\left[1+\left(Ax\right)^2\right]\right\} \qquad (B4b)$$

$$I_{\text{Disk}_d,z} = I_{\text{disk},z} + m_{\text{disk}}d^2 = \frac{1}{4}\rho\pi r^4\cos\left(\tan^{-1}\frac{1}{2Ax}\right)^2 + \rho\pi r^2 x^2$$
$$= \rho\pi r^2\left[\frac{1}{4}r^2\cos\left(\tan^{-1}\frac{1}{2Ax}\right)^2 + x^2\right] \qquad (B4c)$$

Additional Steps to Set Up the Integral of Disks over the Whole Whisker Length

Equations B3 and *B4* express the mass moment of inertia for each differential cross-section, but both still contain the variable *r*, which must be replaced with a function of *x* to perform the integration. There are thus a few additional steps before the integral is set up over the length of the whisker.

Although the integral will be calculated with respect to *x*, whisker geometry is described in terms of the arc length, which curves relative to the *x*-axis. The relationship between the *x*-coordinate along a whisker and the arc length coordinate $L(x)$ is shown in *Eq. B5*:

$$L(x) = \int_0^x \sqrt{1 + z'(x)^2}dx = \int_0^x \sqrt{1 + (2Ax)^2}dx$$
$$= \frac{1}{2}x\sqrt{1 + 4A^2x^2} + \frac{\sinh^{-1}(2Ax)}{4A}. \quad (B5)$$

The cross-sectional radius of the whisker, r, can now be expressed in terms of $r(L(x))$, as a function of x at that location.

When the base diameter of the whisker is R_{Base}, the tip dimeter is zero, and the total arc length is S_{Total}, the radius $r(L)$ at a given point L along the arc length can be found by *Eq. B6*:

$$r(L) = R_{Base} - \frac{R_{Base}L}{S_{Total}}. \quad (B6)$$

Substituting L in *Eq. B6* into *Eq. B5*:

$$r(x) = R_{Base} - \frac{R_{Base}}{S_{Total}}\left[\frac{1}{2}x\sqrt{1 + 4A^2x^2} + \frac{\sinh^{-1}(2Ax)}{4A}\right]. \quad (B7)$$

Finally, substituting *Eq. B7* into *Eq. B4* yields I_{Disk_d} expressed only as a function of x.

Integrating Unit Cross-Sectional I_{Mass} over the Entire Whisker

Now that the unit mass moment of inertia, $I_{Dist\_d}(x)$, is a function of only one variable, x, the limits of the integral can then be set from whisker base ($x = 0$) to tip ($x = x_f$). The upper limit, x_f, can be obtained numerically from *Eq. B5* when x and L are replaced with x_f and S_{Total}, respectively.

By integrating the unit mass moment of inertia with respect to x, I_{Mass} of the entire whisker can be found:

$$I_{Mass}(x) = \int_0^{xf} I_{Disk\_d}(x)dx. \quad (B8)$$

Mathematica was unable to solve *Eq. B8* analytically but was able to solve it numerically.

Generally, for a curved whisker, the smallest value for I_{Mass} is for rotation about the x-axis because it has the least amount of material distributed from the axis of rotation. The value for I_{Mass} for rotation about the y-axis is larger than for rotation about the z-axis because the distance of a given point mass along the whisker from the y-axis is $\sqrt{x^2+z^2}$, whereas from the z-axis it is x.

Convergence of the Two Mass Moments of Inertia of a Whisker Derived Using Two Different Approaches

To validate the two different computational approaches described in APPENDIX A and APPENDIX B, we examined the special case of a whisker with negligible intrinsic curvature and a single slope. The two approaches should converge to the same solution for this special case.

The parameters used were curvature coefficient $A \approx 0$/mm (note that the integrand would be nonexistent by definition if A were exactly 0), density $\rho = 1$ mg/mm^3, arc length $S_{Total} = 35$ mm, and base diameter $R_{Base} = 0.1$ mm.

The value of I_{Mass} computed using the superposition approach in APPENDIX A yields 44.8986 mg·mm^2 about the z-axis, whereas the disk-integral approach of APPENDIX B yields 44.8991 for rotation about the z-axis and 44.8986 about the y-axis. The relative error between the two approaches is $<0.00012\%$. In addition, APPENDIX B yields a negligible value of I_{Mass} about the x-axis, $1.57e^{-34}$, which is expected for a straight whisker.

Finally, we performed a sensitivity analysis to assess the effect of varying R_{Base} and S_{Total} on the error between the superposition and disk-integral approaches.

Within an anatomically plausible range, error increases as R_{Base} increases and/or as S_{Total} decreases. These changes in error are expected if the whisker is divided into the same number of differential disks. The reason is that each differential disk cross-section is approximated as uniform, but as the whisker becomes shorter and thicker, this approximation becomes less valid.

ACKNOWLEDGMENTS

We thank Dr. Chris S. Bresee and Prof. J. W. Rudnicki for many helpful discussions.

Present address of H. M. Belli: Dept. of Population Health, Biostatistics Div., New York Univ. Langone Health, New York, NY 10016.

GRANTS

This work was supported by a series of grants: initially by National Science Foundation Awards CAREER IOS-0846088 and then EFRI-0938007 and finally by National Institute of Neurological Disorders and Stroke Grant R01-NS-091439 to M. J. Z. Hartmann. H. M. Belli was supported, in part, by Ruth L. Kirschstein National Research Service Award Individual Predoctoral Fellowship F31-NS-090872-01A1 and by an NIH TL1 Clinical and Translational Postdoctoral Fellowship, 5TL1TR001447-04.

DISCLOSURES

No conflicts of interest, financial or otherwise, are declared by the authors.

AUTHOR CONTRIBUTIONS

A.E.-T.Y., H.M.B., and M.J.Z.H. conceived and designed research; A.E.-T.Y. performed experiments; A.E.-T.Y. and M.J.Z.H. analyzed data; A.E.-T.Y., H.M.B., and M.J.Z.H. interpreted results of experiments; A.E.-T.Y. and M.J.Z.H. prepared figures; A.E.-T.Y. and M.J.Z.H. drafted manuscript; A.E.-T.Y., H.M.B., and M.J.Z.H. edited and revised manuscript; A.E.-T.Y., H.M.B., and M.J.Z.H. approved final version of manuscript.

REFERENCES

Adineh VR, Liu B, Rajan R, Yan W, Fu J. Multidimensional characterisation of biomechanical structures by combining Atomic Force Microscopy and Focused Ion Beam: a study of the rat whisker. *Acta Biomater* 21: 132–141, 2015. doi:10.1016/j.actbio.2015.03.028.

Ahissar E, Kleinfeld D. Closed-loop neuronal computations: focus on vibrissa somatosensation in rat. *Cereb Cortex* 13: 53–62, 2003. doi:10.1093/cercor/13.1.53.

Ahissar E, Knutsen PM. Object localization with whiskers. *Biol Cybern* 98: 449–458, 2008. doi:10.1007/s00422-008-0214-4.

Ahl AS. The role of vibrissae in behavior: a status review. *Vet Res Commun* 10: 245–268, 1986. doi:10.1007/BF02213989.

Bagdasarian K, Szwed M, Knutsen PM, Deutsch D, Derdikman D, Pietr M, Simony E, Ahissar E. Pre-neuronal morphological processing of object location by individual whiskers. *Nat Neurosci* 16: 622–631, 2013. doi:10.1038/nn.3378.

Belli HM, Yang AE, Bresee CS, Hartmann MJ. Variations in vibrissal geometry across the rat mystacial pad: base diameter, medulla, and taper. *J Neurophysiol* 117: 1807–1820, 2017. doi:10.1152/jn.00054.2016.

Berg RW, Kleinfeld D. Rhythmic whisking by rat: retraction as well as protraction of the vibrissae is under active muscular control. *J Neurophysiol* 89: 104–117, 2003. doi:10.1152/jn.00600.2002.

Birdwell JA, Solomon JH, Thajchayapong M, Taylor MA, Cheely M, Towal RB, Conradt J, Hartmann MJ. Biomechanical models for radial distance determination by the rat vibrissal system. *J Neurophysiol* 98: 2439–2455, 2007. doi:10.1152/jn.00707.2006.

Bosman LW, Houweling AR, Owens CB, Tanke N, Shevchouk OT, Rahmati N, Teunissen WH, Ju C, Gong W, Koekkoek SK, De Zeeuw CI. Anatomical pathways involved in generating and sensing rhythmic whisker movements. *Front Integr Nuerosci* 5: 53, 2011. doi:10.3389/fnint.2011.00053.

Boubenec Y, Shulz DE, Debrégeas G. Whisker encoding of mechanical events during active tactile exploration. *Front Behav Neurosci* 6: 74, 2012. doi:10.3389/fnbeh.2012.00074.

Brecht M, Preilowski B, Merzenich MM. Functional architecture of the mystacial vibrissae. *Behav Brain Res* 84: 81–97, 1997. doi:10.1016/S0166-4328(97)83328-1.

Bush NE, Schroeder CL, Hobbs JA, Yang AE, Huet LA, Solla SA, Hartmann MJ. Decoupling kinematics and mechanics reveals coding properties of trigeminal ganglion neurons in the rat vibrissal system. *eLife* 5: e13969, 2016a. doi:10.7554/eLife.13969.

Bush NE, Solla SA, Hartmann MJ. Whisking mechanics and active sensing. *Curr Opin Neurobiol* 40: 178–188, 2016b. doi:10.1016/j.conb.2016.08.001.

Carvell GE, Simons DJ. Biometric analyses of vibrissal tactile discrimination in the rat. *J Neurosci* 10: 2638–2648, 1990. doi:10.1523/JNEUROSCI.10-08-02638.1990.

Chernova OF. [Architectonic and diagnostic significance of hair cortex and medulla]. *Izv Akad Nauk Ser Biol* 30: 63–73, 2003.

Diamond ME. Texture sensation through the fingertips and the whiskers. *Curr Opin Neurobiol* 20: 319–327, 2010. doi:10.1016/j.conb.2010.03.004.

Guić-Robles E, Valdivieso C, Guajardo G. Rats can learn a roughness discrimination using only their vibrissal system. *Behav Brain Res* 31: 285–289, 1989. doi:10.1016/0166-4328(89)90011-9.

Haidarliu S, Bagdasarian K, Shinde N, Ahissar E. Muscular basis of whisker torsion in mice and rats. *Anat Rec (Hoboken)* 300: 1643–1653, 2017. doi:10.1002/ar.23623.

Haidarliu S, Golomb D, Kleinfeld D, Ahissar E. Dorsorostral snout muscles in the rat subserve coordinated movement for whisking and sniffing. *Anat Rec (Hoboken)* 295: 1181–1191, 2012. doi:10.1002/ar.22501.

Haidarliu S, Kleinfeld D, Ahissar E. Mediation of muscular control of rhinarial motility in rats by the nasal cartilaginous skeleton. *Anat Rec (Hoboken)* 296: 1821–1832, 2013. doi:10.1002/ar.22822.

Haidarliu S, Simony E, Golomb D, Ahissar E. Collagenous skeleton of the rat mystacial pad. *Anat Rec (Hoboken)* 294: 764–773, 2011. doi:10.1002/ar.21371.

Haidarliu S, Simony E, Golomb D, Ahissar E. Muscle architecture in the mystacial pad of the rat. *Anat Rec (Hoboken)* 293: 1192–1206, 2010. doi:10.1002/ar.21156.

Hartmann M. Vibrissa mechanical properties. *Scholarpedia* 10: 6636, 2015. doi:10.4249/scholarpedia.6636.

Hausman LA. Recent studies of hair structure relationships. *Sci Mon* 30: 258–278, 1930.

Hibbeler RC. *Mechanics of Materials*. Boston, MA: Prentice Hall, 2014.

Hill DN, Bermejo R, Zeigler HP, Kleinfeld D. Biomechanics of the vibrissa motor plant in rat: rhythmic whisking consists of triphasic neuromuscular activity. *J Neurosci* 28: 3438–3455, 2008. doi:10.1523/JNEUROSCI.5008-07.2008.

Hires SA, Pammer L, Svoboda K, Golomb D. Tapered whiskers are required for active tactile sensation. *eLife* 2: e01350, 2013. doi:10.7554/eLife.01350.

Hires SA, Schuyler A, Sy J, Huang V, Wyche I, Wang X, Golomb D. Beyond cones: an improved model of whisker bending based on measured mechanics and tapering. *J Neurophysiol* 116: 812–824, 2016. doi:10.1152/jn.00511.2015.

Hobbs JA, Towal RB, Hartmann MJ. Probability distributions of whisker-surface contact: quantifying elements of the rat vibrissotactile natural scene. *J Exp Biol* 218: 2551–2562, 2015. doi:10.1242/jeb.116186.

Hobbs JA, Towal RB, Hartmann MJ. Spatiotemporal patterns of contact across the rat vibrissal array during exploratory behavior. *Front Behav Neurosci* 9: 356, 2016. doi:10.3389/fnbeh.2015.00356.

Huet LA, Hartmann MJ. Simulations of a vibrissa slipping along a straight edge and an analysis of frictional effects during whisking. *IEEE Trans Haptics* 9: 158–169, 2016. doi:10.1109/TOH.2016.2522432.

Huet LA, Hartmann MJ. The search space of the rat during whisking behavior. *J Exp Biol* 217: 3365–3376, 2014. doi:10.1242/jeb.105338.

Huet LA, Schroeder CL, Hartmann MJ. Tactile signals transmitted by the vibrissa during active whisking behavior. *J Neurophysiol* 113: 3511–3518, 2015. doi:10.1152/jn.00011.2015.

Ibrahim L, Wright EA. The growth of rats and mice vibrissae under normal and some abnormal conditions. *J Embryol Exp Morphol* 33: 831–844, 1975.

Kan QH, Rajan R, Fu J, Kang GZ, Yan WY. Elastic modulus of rat whiskers–a key biomaterial in the rat whisker sensory system. *Mater Res Bull* 48: 5026–5032, 2013. doi:10.1016/j.materresbull.2013.04.070.

Kaneko M, Kanayama N, Tsuji T. Active antenna for contact sensing. *IEEE Trans Rob Autom* 14: 278–291, 1998. doi:10.1109/70.681246.

Khatri V, Bermejo R, Brumberg JC, Zeigler HP. Whisking in air: encoding of kinematics by VPM neurons in awake rats. *Somatosens Mot Res* 27: 111–120, 2010. doi:10.3109/08990220.2010.502381.

Kim D, Moller R. Biomimetic whiskers for shape recognition. *Rob Auton Syst* 55: 229–243, 2007. doi:10.1016/j.robot.2006.08.001.

Knutsen PM, Biess A, Ahissar E. Vibrissal kinematics in 3D: tight coupling of azimuth, elevation, and torsion across different whisking modes. *Neuron* 59: 35–42, 2008. doi:10.1016/j.neuron.2008.05.013.

Knutsen PM, Pietr M, Ahissar E. Haptic object localization in the vibrissal system: behavior and performance. *J Neurosci* 26: 8451–8464, 2006. doi:10.1523/JNEUROSCI.1516-06.2006.

Lucianna FA, Albarracín AL, Vrech SM, Farfán FD, Felice CJ. The mathematical whisker: a review of numerical models of the rat's vibrissa biomechanics. *J Biomech* 49: 2007–2014, 2016. doi:10.1016/j.jbiomech.2016.05.019.

O'Connor DH, Hires SA, Guo ZV, Li N, Yu J, Sun QQ, Huber D, Svoboda K. Neural coding during active somatosensation revealed using illusory touch. *Nat Neurosci* 16: 958–965, 2013. doi:10.1038/nn.3419.

Oatis CA. *Kinesiology: The Mechanics and Pathomechanics of Human Movement*. Philadelphia, PA: Lippincott Williams & Wilkins, 2004.

Polley DB, Rickert JL, Frostig RD. Whisker-based discrimination of object orientation determined with a rapid training paradigm. *Neurobiol Learn Mem* 83: 134–142, 2005. doi:10.1016/j.nlm.2004.10.005.

Quist BW, Faruqi RA, Hartmann MJ. Variation in Young's modulus along the length of a rat vibrissa. *J Biomech* 44: 2775–2781, 2011. doi:10.1016/j.jbiomech.2011.08.027.

Quist BW, Hartmann MJ. Mechanical signals at the base of a rat vibrissa: the effect of intrinsic vibrissa curvature and implications for tactile exploration. *J Neurophysiol* 107: 2298–2312, 2012. doi:10.1152/jn.00372.2011.

Quist BW, Seghete V, Huet LA, Murphey TD, Hartmann MJ. Modeling forces and moments at the base of a rat vibrissa during noncontact whisking and whisking against an object. *J Neurosci* 34: 9828–9844, 2014. doi:10.1523/JNEUROSCI.1707-12.2014.

Simony E, Bagdasarian K, Herfst L, Brecht M, Ahissar E, Golomb D. Temporal and spatial characteristics of vibrissa responses to motor commands. *J Neurosci* 30: 8935–8952, 2010. doi:10.1523/JNEUROSCI.0172-10.2010.

Solomon JH, Hartmann MJ. Artificial whiskers suitable for array implementation: accounting for lateral slip and surface friction. *IEEE Trans Robot* 24: 1157–1167, 2008. doi:10.1109/TRO.2008.2002562.

Solomon JH, Hartmann MJ. Biomechanics: robotic whiskers used to sense features. *Nature* 443: 525, 2006. doi:10.1038/443525a.

Solomon JH, Hartmann MJ. Extracting object contours with the sweep of a robotic whisker using torque information. *Int J Rob Res* 29: 1233–1245, 2010. doi:10.1177/0278364908104468.

Solomon JH, Hartmann MJ. Radial distance determination in the rat vibrissal system and the effects of Weber's law. *Philos Trans R Soc Lond B Biol Sci* 366: 3049–3057, 2011. doi:10.1098/rstb.2011.0166.

Stanić V, Bettini J, Montoro FE, Stein A, Evans-Lutterodt K. Local structure of human hair spatially resolved by sub-micron X-ray beam. *Sci Rep* 5: 17347, 2015. doi:10.1038/srep17347.

Thé L, Wallace ML, Chen CH, Chorev E, Brecht M. Structure, function, and cortical representation of the rat submandibular whisker trident. *J Neurosci* 33: 4815–4824, 2013. doi:10.1523/JNEUROSCI.4770-12.2013.

Towal RB, Quist BW, Gopal V, Solomon JH, Hartmann MJ. The morphology of the rat vibrissal array: a model for quantifying spatiotemporal patterns of whisker-object contact. *PLoS Comput Biol* 7: e1001120, 2011. doi:10.1371/journal.pcbi.1001120.

Ueno N, Svinin MM, Kaneko M. Dynamic contact sensing by flexible beam. *IEEE/ASME Trans Mechatron* 3: 254–264, 1998. doi:10.1109/3516.736160.

Vaxenburg R, Wyche I, Svoboda K, Efros AL, Hires SA. Dynamic cues for whisker-based object localization: an analytical solution to vibration during active whisker touch. *PLoS Comput Biol* 14: e1006032, 2018. doi:10.1371/journal.pcbi.1006032.

Vincent SB. *The Function of the Vibrissae in the Behavior of the White Rat* (PhD dissertation). Chicago, IL: Univ. of Chicago, 1912.

Voges D, Carl K, Klauer GJ, Uhlig R, Schilling C, Behn C, Witte H. Structural characterization of the whisker system of the rat. *IEEE Sens J* 12: 332–339, 2012. doi:10.1109/JSEN.2011.2161464.

Welker WI. Analysis of sniffing of the albino rat. *Behaviour* 22: 223–244, 1964. doi:10.1163/156853964X00030.

Williams CM, Kramer EM. The advantages of a tapered whisker. *PLoS One* 5: e8806, 2010. doi:10.1371/journal.pone.0008806.

Wineski LE. Movements of the cranial vibrissae in the Golden hamster (*Mesocricetus auratus*). *J Zool* 200: 261–280, 1983. doi:10.1111/j.1469-7998.1983.tb05788.x.

Yang AE, Hartmann MJ. Whisking kinematics enables object localization in head-centered coordinates based on tactile information from a single vibrissa. *Front Behav Neurosci* 10: 145, 2016. doi:10.3389/fnbeh.2016.00145.